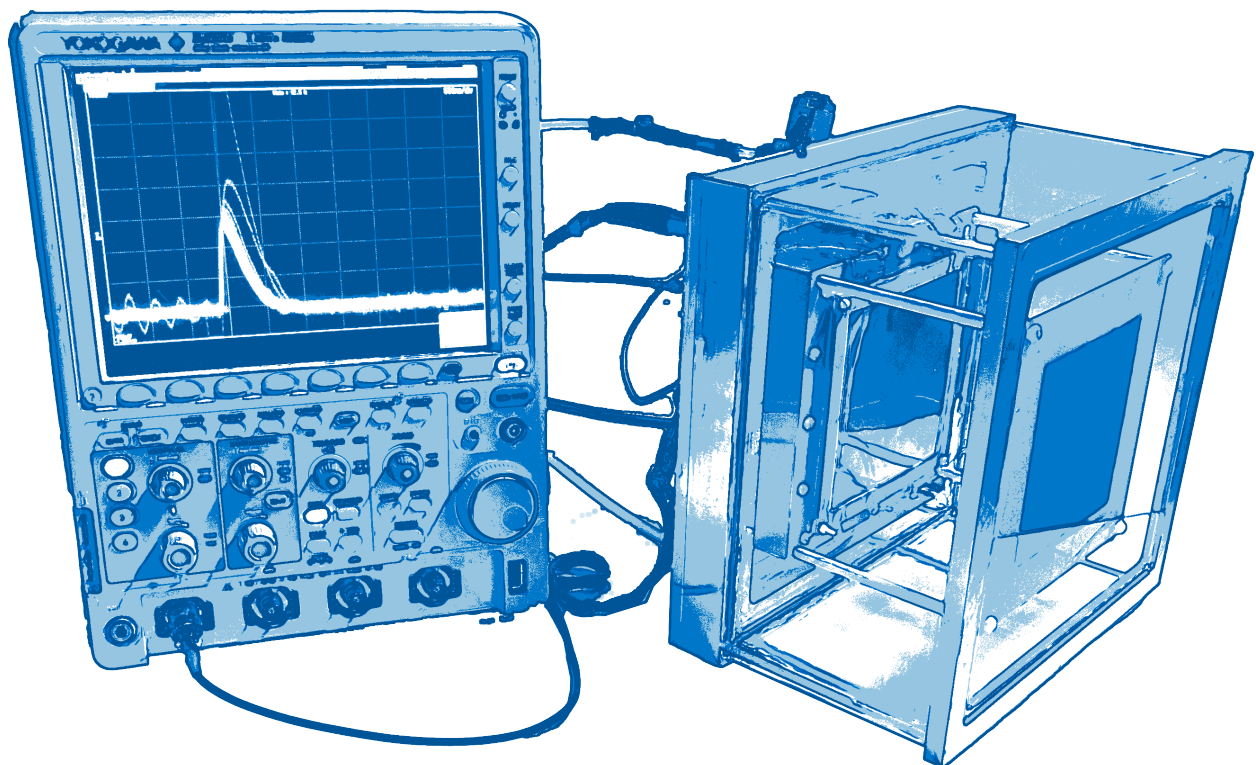


Bachelor's Thesis

Design and construction of a  
gaseous detector readout system  
for use in education and  
science-outreach

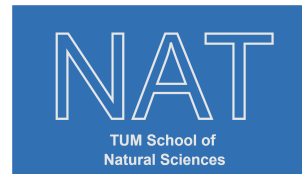
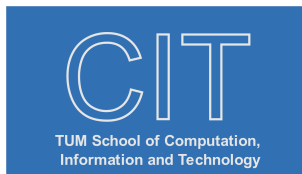
Oguz Alp Duran







TECHNISCHE UNIVERSITÄT MÜNCHEN



# Design and construction of a gaseous detector readout system for use in education and science-outreach

## Entwurf und Bau eines Auslesesystems für Gasdetektoren für Lehre und Science-Outreach

Bachelor's Thesis

**Author:** Oguz Alp Duran  
**Examiner:** Prof. Dr. Gabriele Schrag, Prof. Dr. Laura Fabbietti  
**Supervisor:** Berkin Ulukutlu  
**Date:** June 18, 2024



I confirm that the results presented in this master's thesis is my own work and I have documented all sources and materials used.

Ich versichere, dass ich diese Masterarbeit selbstständig verfasst und nur die angegebenen Quellen und Hilfsmittel verwendet habe.

Munich, June 18, 2024

Oguz Alp Duran



# Abstract

Over the past fifty years, particle and nuclear physics have made significant advancements, driven by innovations in particle detection and measurement technologies. Modern experiments utilize cutting-edge tools such as MAPS and MPGD devices, coupled with advanced readout electronics. However, in the context of science outreach and education, more traditional detector methods, like cloud chambers, are still utilized. This thesis aims to bridge this technological gap by constructing a cost-effective yet efficient particle detector based on 10x10 cm<sup>2</sup> area GEMs. The detector design incorporates inexpensive off-the-shelf components for the front-end electronics and utilizes Arduino microcontrollers and Raspberry Pi computers for the digital readout system.

The analog front-end circuitry features an amplification stage followed by a comparator, enabling Time-Over-Threshold-based measurements of the energy loss of incident charged particles. This thesis details the considerations for the circuitry, supported by simulations and measurements using prototype readout boards. Additionally, a 64-channel modular version of the readout card system, necessary for 2D particle tracking, is presented and discussed.

The constructed detector system is intended for use in science education with high school students as part of the ORIGINS Go-To-School program later this year.



# Contents

<b>1</b>	<b>Introduction</b>	<b>9</b>
1.1	From CERN to TPC . . . . .	9
1.2	Gaseous Electron Multipliers (GEM) . . . . .	10
1.3	Time Projection Chamber (TPC) . . . . .	11
1.3.1	State of the Art Readout Electronics . . . . .	11
1.4	Outreach . . . . .	12
1.5	Our GEM Based Detector . . . . .	13
<b>2</b>	<b>Theoretical Background</b>	<b>15</b>
2.1	Working Principle: GEM . . . . .	15
2.1.1	Ionization Detectors . . . . .	15
2.1.2	Electron Avalanche . . . . .	16
2.2	Signal Generation . . . . .	17
2.2.1	Induction . . . . .	17
2.2.2	Signal Time Shaping . . . . .	17
2.3	Working Principle: Operational Amplifiers (OPAMP) . . . . .	19
2.3.1	Configuration . . . . .	20
2.3.2	Noise . . . . .	23
2.3.3	AC-Coupling . . . . .	23
2.4	Working Principle: Comparators . . . . .	24
2.5	Working Principle: Digitization . . . . .	24
2.5.1	Time over Threshold (ToT) . . . . .	25
<b>3</b>	<b>Simulations</b>	<b>27</b>
3.1	Pre-amplifier and AC-Coupling . . . . .	27
3.1.1	Integrator . . . . .	27
3.1.2	Negative Gain Amplifier . . . . .	27
3.2	AC-Coupling . . . . .	28
3.3	Comparator . . . . .	29
<b>4</b>	<b>Implementation</b>	<b>31</b>
4.1	OPAMP Gain Method . . . . .	31
4.1.1	AC-Coupling . . . . .	35
4.1.2	Comparator . . . . .	35

4.2	Digitization . . . . .	36
4.2.1	Arduino Studies . . . . .	36
4.2.2	Mono-stable and the Binary Hit Mode . . . . .	38
4.3	One channel to Multiple Channels . . . . .	39
4.4	PCB Layers and Description . . . . .	44
<b>5</b>	<b>Summary and Outlook</b> . . . . .	<b>47</b>
5.1	Outlook . . . . .	48
5.2	Acknowledgments . . . . .	48

# Chapter 1

## Introduction

Pushing the boundaries of fundamental physics research requires solutions pushing the boundaries of engineering, where the practical meets the theoretical - or the imagination. This thesis will explain our steps to read out a gaseous detector.

### 1.1 From CERN to TPC

CERN, *Conseil européen pour la recherche nucléaire* (french. European Organization for Nuclear Research) is an institute having roots well within the 20th century aiming towards a common and accessible place for international scale fundamental research to take place. Here, scientists sought ways to explain, describe, and quantify how our universe worked.

An essential tool for us to categorize and quantize measurements resulting from the experiments at CERN happened through so-called detectors.

<p><i>(Measurement)</i> <b>Detector:</b> <i>as in sensor</i>, a device that detects some <u>physical quantity</u> and responds usually with a <u>transmitted signal</u>.</p>
--

*(As submitted to the Merriam-Webster Dictionary)*

Using this definition, one expects a measurement result from a detector to have quantifiable outputs within electronic means. This was not the case during the early infancy of CERN [1]. Human labor was required to extract the data; even well-trained eyes made mistakes and overlooked much information in the bubble chambers.

One potential improvement was electrical circuits, as radio and the vacuum tube emerged into our lives. Being at the forefront of research, CERN used these technologies very thoroughly. Though not the first to do so [2], a notable amount of research went to acquisition electronics. It enabled scientists to numerically represent and store the acquired data. Now, the era of siphoning datum out of detectors and processing them in mind-boggling man-made automatons was to begin. **After all, the power was in the numbers.**

## 1.2 Gaseous Electron Multipliers (GEM)

Subsequent developments in gaseous detectors, such as the multi-wire proportional chamber (MWPC) developed by Charpak, who received the Nobel Prize in 1992, brought many possibilities for particle research. Gas chambers realized their potential as detectors by using a well-known effect first described by John S. Townsend circa 1897 by the self-titled Townsend Avalanche [3]. It occurs when ionized particles expel electrons, which then accelerate under the influence of an electric field. These electrons collide with nearby gas molecules, and upon reaching the critical ionization energy of the gas, they release more electrons. Each collision results in further scattering and the generation of additional electrons, effectively multiplying the number of electrons through this chain of collisions.

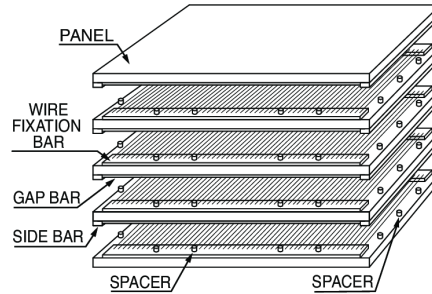


Figure 1.1: Stacked configuration of a MWPC used for fundamental particle research at the LHCb experiment at CERN. It consists of wires suspended in air and non-conductive plates under them. Via the wires, a well-defined electrical field is generated, which uses the Townsend Avalanche to generate electrons almost at the surface of the wires, thus creating a signal via the avalanche. [4].

Sauli developed his MWPC using the above-described principle, but one issue needed to be addressed. This issue stemmed from the engineering and manufacturing of said detectors. The principles of working were clear, but the manufacturing needed to be more convenient. Turning to printable circuit board-like material processing, Sauli invented the GEM. Such a GEM consists of small, well-defined, etched polyamide holes. We shall describe the inner workings of a singular GEM and the entire system, including how the signal forms and the path an electron takes until it hits a collection pad.

Nonetheless, it is safe to say Sauli and his colleagues indeed started an avalanche<sup>1</sup> of novel detection systems based on simple<sup>2</sup> electromagnetic principles such as drift and ionization **which are still used in experiments at CERN.**

<sup>1</sup>Pun intended.

<sup>2</sup>It seems too obvious retrospectively; however, we must not forget it was non-trivial back then.

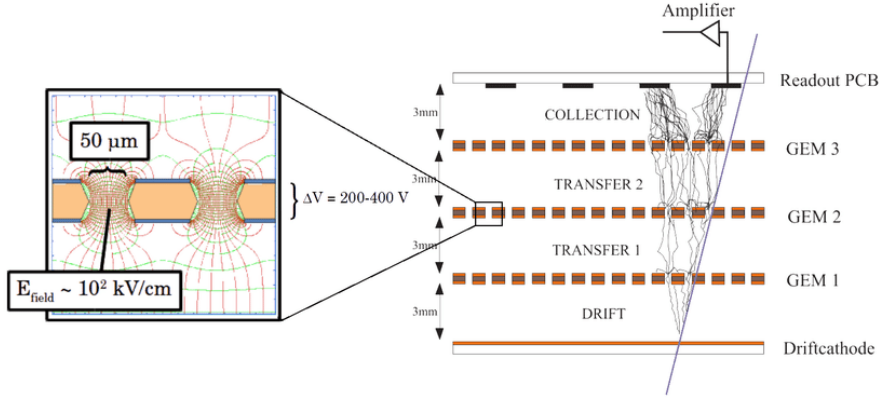


Figure 1.2: Schematics of a triple stacked GEM detector. Left, Electric field configuration within the GEM's holes. Right, the entire GEM stack as well as collection electrodes for electrons and ions respectively falling on an anode and a cathode. [5].

## 1.3 Time Projection Chamber (TPC)

The TPC was born out of the necessity of having a large volume and having this volume have an unprecedented three-dimensional spatial resolution. Combining a 2-D planar amplification chamber (here GEM) for x/y coordinates and the total drifting time the charge needs to reach the readout for the z coordinate was the solution. Thus, an excellent timing resolution was required.

### 1.3.1 State of the Art Readout Electronics

Needs for a fast and reliable readout method were imminent at ALICE TPC [6, 7]. It used the MWPC before its upgrade to a GEM-based readout. One peculiar challenge with GEM readout was the need for continuous readout of the channels, which enabled unprecedented data throughput about the particle collision. Thus, the serialized analog-digital multipurpose application-specific integrated circuit (SAMPA) was born. It contains a continuous 32-channel readout for the anode of the GEM, taking much less space than normal approaches via off-the-shelf IC and PCB approaches. [8] [7]

As seen in the figure above, the SAMPA chip's signal processing chain consists of a charge-sensitive amplifier, a pole-zero cancellation network tuned to the amplifier topology, a Gaussian pulse shaper, and a non-inverting stage (NIS). Such ASIC design is quite expensive in terms of human resources. They require special knowledge of solid-state physics and production processes. It also means smaller production nodes, resulting in premium prices for low-yield production.

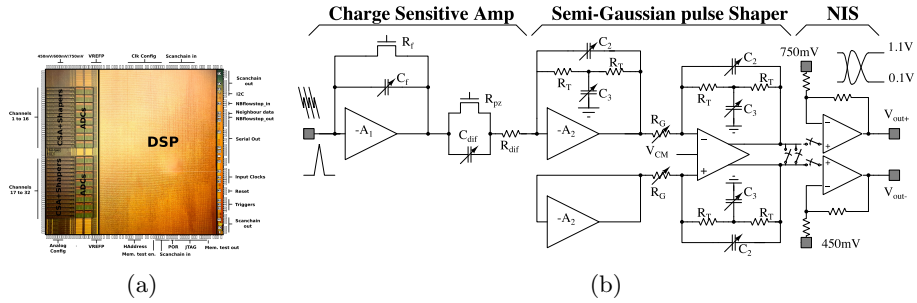


Figure 1.3: (a), SAMPA Chip Die Shot and (b), Internal structure of the singular SAMPA signal processing channel. Figures from [8]

## 1.4 Outreach

Nowadays, science requires an immense collaboration with thousands of people working towards a shared goal in a project to understand our universe better. For example, a steady growth of people studying engineering and physics is needed. To ensure this, children and teenagers must be motivated by the latest physics research themes. For this, many approaches were made, be it a cloud chamber or the silicon-based Cosmic Pi<sup>3</sup>, by European institutes. However, these approaches follow the current trends in high-energy particle physics by a decade behind. Having motivated our approach to the GEM-based detectors and the importance of ALICE's new GEM-based TPC, we believe that a new outreach method needs to be theorized. Herewith, we will use our GEM chamber for the following points of contact for students to know and like science-related topics:

Our detector will be presented by us, engineers, and scientists in the field of research. This will first provide an invaluable experience of talking to an expert at such an early stage of the pupil's career. We aim to be role models and induce excitement for discovering mother nature. Another point where the outreach project will shine is showing the collaborative effort of many people from different fields to produce a tangible result, such as our GEM-based detector. Secondly, the hands-on experience of seeing, plugging in, adjusting the detector, and retrieving and analyzing the data it provides will also make the subject more approachable and easier to understand the concepts we will introduce to them.

This project will not only serve didactic purposes. It will also serve as a first contact point for students to see how engineering is done, namely how to approach theoretical concepts and solve problems that arise when implementing it pragmatically while supporting rational and logical thinking. It will also introduce many foreign and advanced topics in physics. These topics range from the GEM detector, which vividly demonstrates how particles are detected and tracked, to concepts like ionization, electron multiplication, signal processing,

<sup>3</sup>CERN's affordable cosmic ray counter.

and many more.

In a nutshell, we hope to provide unique learning experience that brings theory and practice together, which develops critical skills, and inspires students to study in engineering and physics. This idea will be supported by the "Go-to-schools" ORIGINS Excellence Cluster <sup>4</sup>, a collaborative effort of TUM, Ludig Maximillian University and the Max Planck Institutes.

## 1.5 Our GEM Based Detector

Every readout needs a detector. Our detector's geometry is straightforward and pleasing to look at. The detector body in figure 1.4 consists of several main

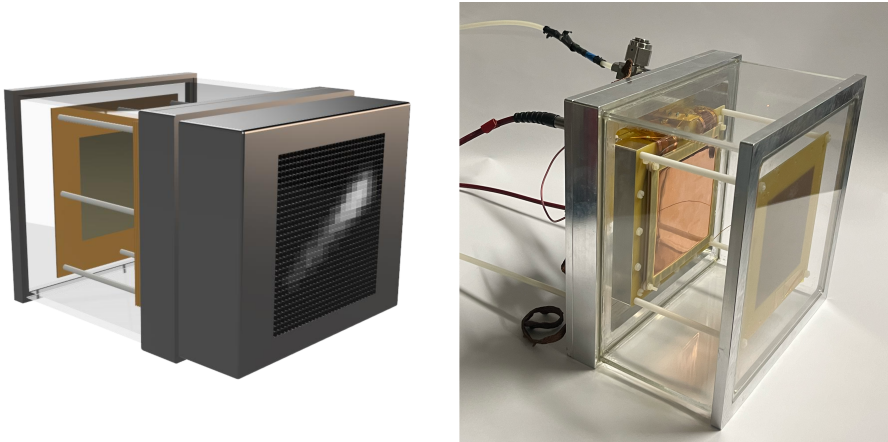


Figure 1.4: Left, render of the to-be-produced GEM-based detector; right, the detector we produced.

parts- the most prominent being the drift chamber inside the gas vessel. The gas vessel is a hermetically sealed ensemble of machined blocks of aluminum and glass. The glass side windows allow the detector's guts to be seen outside. This enables two main things: the vessel is free to be observed, and this enables us to explain how phenomena like drift occur while being able to show parts of the detector directly, and if discharges between the amplifying GEM foils occur, the discharges are to be seen visually. The most exciting part inside the gas vessel is the GEM stack, which amplifies the electrons incident from ionized gas. Not to forget the bias tree that supplies the correct bias voltage to the GEMs. These GEMs are placed 2mm apart, a number gained from practical experiences by the ALICE TPC. The GEMs have two sides: a functional bottom and top layer. These layers are then put under a constant voltage provided by the voltage divider resistor circuit within the chamber. The biasing voltages were obtained using simulations with a tool called Garfield++, together with

<sup>4</sup><https://www.origins-cluster.de/>

field maps generated in COMSOL Multiphysics. These numbers are the result of labor done by Bugia's bachelor thesis [9].

Last but not least, the vessel is closed off with a PCB containing 12.5mmx12.5mm copper pads facing inside the chamber. The copper pads are also connected with vias to the back of the PCB, which houses four 16-pin female pin headers where our design was planned to be slotted in.

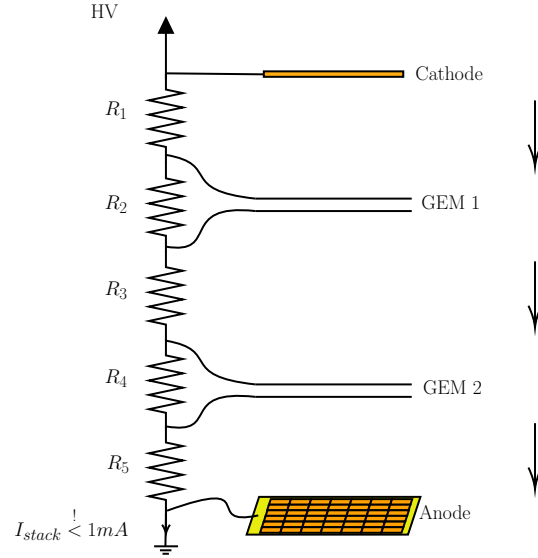


Figure 1.5: The current GEM stack inside the vacuum vessel and the resistor chain for biasing the GEMs and the drift fields. Values can be taken from table 1.1.

Table 1.1: Table of resistances for the voltage divider and provided voltages and the electric fields resulting.

Resistor	Resistance[MΩ]	Node	Voltage [V]	Field Name	E-Field [V/cm]
-	-	Cathode	3920	Drift	340.6
$R_1$	4.7	GEM1 Top	2200	GEM1	468.09
$R_2$	1	GEM1 Bottom	1731.9	GEM1	2340.43
$R_3$	1.5	GEM2 Top	1029.7	Transfer	468.09
$R_4$	1	GEM2 Bottom	561.7	GEM2	2246.81
$R_5$	1.2	Anode	0	Induction	-

## Chapter 2

# Theoretical Background

### 2.1 Working Principle: GEM

As mentioned in the introduction, GEMs are used extensively in cutting-edge research. Let us now understand how they tick inside.

#### 2.1.1 Ionization Detectors

The most simple ionization detector is the Geiger-Müller Tube, widely used in Geiger Counters since its discovery in the atomic era. These detectors are mainly used for dosimetry. The most essential part consists of a coaxial arrangement of cavity and wire.

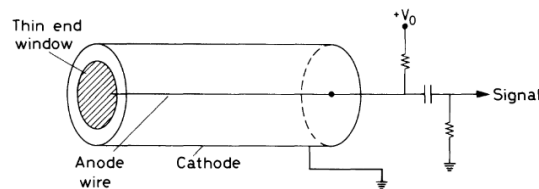


Figure 2.1: Basic construction of a Geiger-Müller Tube. The inner wire acts as an anode, and a bias voltage is set in reference to the cathode. [10]

An electric field is formed in such a coaxial electrode arrangement due to the potential difference within. Given a bias of  $V_0$ , a radial field of

$$\vec{E}(r) = \frac{1}{r} \frac{V_0}{\ln(b/a)} \cdot \vec{e}_r \quad (2.1)$$

with  $r$ : radial distance from axis;  $b$ : inside radius of cylinder;  $a$ : radius of central wire thus prevails. [10] If a particle of enough energy- or perhaps an energetic enough photon- passes through the gaseous tube, pairs of ions and electrons are created. Due to the internal field described in equation 2.1, these charged

particles are accelerated towards the electrodes. While ions (*positive*) accelerate towards the lower potential cathode, the negatively charged electrons accelerate towards the anode wire. In such chambers, two types of ionization occur:

1. Primary ionization originated from an external particle;
2. Secondary ionization originated from the accelerated collision products of primary ionization.

### 2.1.2 Electron Avalanche

Since the tubes have sufficient electric fields of a few kilovolts per centimeter, Townsend discharges occur, and electrons gain sufficient energy between collisions with gas molecules to originate secondary ionization. Such an exponential growth is described as the avalanche discharge, thus resulting in an effective gain of an incident ionizing particle.

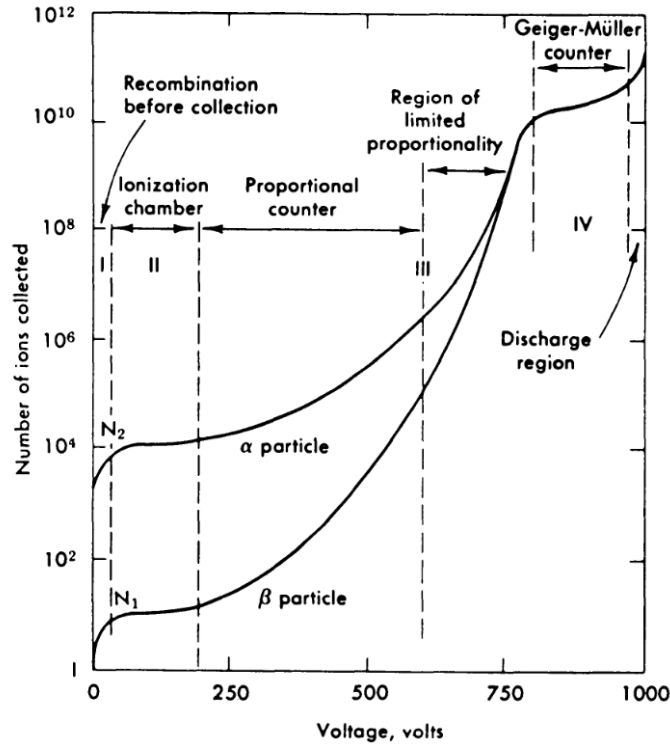


Figure 2.2: Number of ions collected versus the Voltage for a singular wire ionization detector for  $\alpha$  and  $\beta$  particles. [10]

H. Raether studied this gain. [11] Raether described that the gain cannot grow infinitely owing to effects near the anode. When too many electrons are

gathered around the anode, a space charge-like electron cloud is formed, which repels other electrons. This limit is described as approximately  $G = 10^7$  to  $10^8$  depending on the wire diameter. It is easy to lose track of the scale of our Geiger tube. Now, having reached this gain limit, it behaves much more like a streamer discharge conventionally described in electrical engineering. Our area of interest is naturally the region where the most sensitive change to particle types occurs. Thus, the proportional region (seen in figure 2.2) is used widely. A great example is the MWPC used in the original ALICE Time Projection Chamber.

Additionally, despite not working on the exact same principle, our GEMs are being operated in the proportional range seen in figure 2.2, meaning there is an excellent multiplication and also a proportional, thus controllable signal for different particle types.

## 2.2 Signal Generation

Since the avalanche occurs within a few anode wire radii and within a couple of nanoseconds, signals are measured in tens of MHz in speed.

### 2.2.1 Induction

Both anode and cathode are affected via induction due to  $Q$  moving charges. These charges are stored via the capacity formed by the geometry of the detector. Signals are, however, shaped via the internal capacity  $C$  and the resistance of the readout path  $R$ . Which can be described via the following equation systems [12]:

$$I_{pads,total}(t) = \sum_n I_n(t) = \frac{dq(t)}{dt} \quad (2.2)$$

$$= -\frac{q}{V_w} E[x(t)]v(t) \quad (2.3)$$

where  $E[x(t)]$  is the local energy the incoming particle has at a given time  $t$  at location  $x(t)$ , the Voltage given by induction laws at a pad length of  $w$ , and last but not least the  $v(t)$  dependent once again on the particle energy itself [12].

### 2.2.2 Signal Time Shaping

Having established this paradigm of the capacity of the detector body and resistance via the cables, these describe a time constant when the signal reaches approximately 66% of its maximum inhomogeneous allowed Voltage. This constant will play a key role when designing and tuning our amplifier and, thus, our signal path. We can then describe the small signal behavior of said circuit via the standard differential equation system. Constant potentials are (due to differentiation per time being  $dV_{const}/dt = 0$ ) set to ground potential. Using

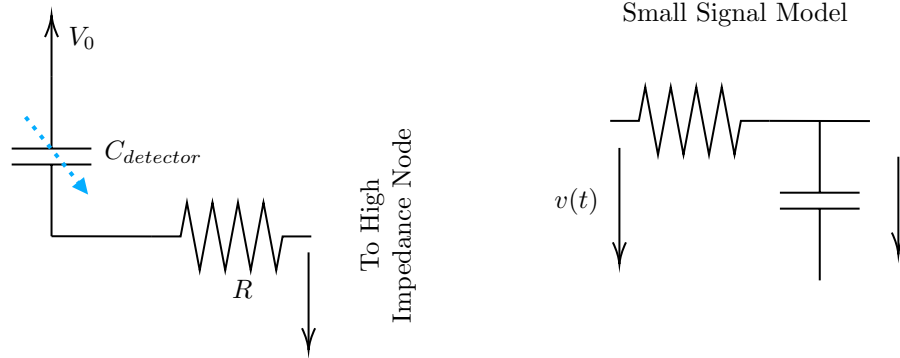


Figure 2.3: Left: Equivalent circuit diagram for the detector body. Right: a small signal model of said circuit with a time-variant small signal produced by the discharge  $v(t)$ .

Kirchoff's Current (KCL) and Voltage Laws (KVL), we can formulate:

$$i_R + i_C = 0 \quad (2.4)$$

$$\frac{v - V_R}{R} + C \frac{dv}{dt} = 0 \quad (2.5)$$

$$\therefore \frac{v}{R} - \frac{V_S}{R} + C \frac{dv}{dt} = 0 \quad (2.6)$$

$$\therefore \frac{V_S}{R} + C \frac{dv}{dt} = \frac{v}{R} \quad (2.7)$$

$$\therefore \frac{dv}{dt} + \frac{dv}{RC} = \frac{V_S}{RC} \quad (2.8)$$

Which indeed looks like an ordinary differential equation with an initial condition of  $v(t = 0) = V_0$ . Let us now solve this ODE. We require two parts, the inhomogeneous and the homogeneous parts, to solve this equation. We can then superimpose these two solutions to get our total system response, i.e.,  $v_{hom} + v_{inh} = v_t$ .

The inhomogeneous part is easy to solve given the input's constant voltage of  $V_S$ . This is our significant signal, which around our small signal is to swing around. This yields the solution in  $t = \infty$  where the capacitor is at the same potential as the considerable signal input- therefore,  $v_{inh} = V_S$

The homogeneous response is more interesting where we set  $V_S$  to zero.

$$\frac{dv}{dt} + \frac{dv}{RC} = 0 \quad (2.9)$$

which is a normal, homogeneous ODE to which we can easily apply our expo-

### 2.3. WORKING PRINCIPLE: OPERATIONAL AMPLIFIERS (OPAMP) 19

nential Ansatz. Ordinarily solving via the Ansatz thus yields:

$$v_{hom} = K_n e^{-t/RC} \quad (2.10)$$

$$\therefore v_t = K_n e^{-t/RC} + V_S \quad (2.11)$$

We only have to determine the  $K_S$  from our initial conditions, which was equal to zero. Solving yields:  $K_n = V_0 - V_S$  and our full solution is then:

$$v_t = V_S + (V_0 - V_S) e^{-t/RC}. \quad (2.12)$$

The exponential term contains an interesting parameter, which is the  $RC = \tau$  parameter we mentioned at the start of this chapter. Assuming a low-frequency device that operates below 200Hz might not perceive the same wire as, say, a circuit operating at 30GHz. This is why engineers had to come up with modeling transmission lines. In the thesis, the impedance along the connection between the readout pads and the amplifier is assumed to be negligible, only providing some thermal noise along with an input capacitor that forms between each stage. This capacitance will be relevant to our amplifier design. Therefore, strict care has been taken in order to decrease the stray capacitance and give the traces a coaxial-like design.

## 2.3 Working Principle: Operational Amplifiers (OPAMP)

As Hans F. Mayer described in his publications about a hundred years ago, [13] we can view the OPAMP as a two-port device with the following characteristics following the European <sup>1</sup> Nullor model.

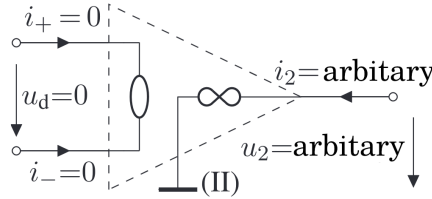


Figure 2.4: The convention followed as a two-port model.

This model is explained with the following equations:

$$\text{OPAMP} \begin{cases} \text{Port 1 } u_1 = 0 & i_{in} = 0 \\ \text{Port 2 } u_2 = \text{arbitrary} & i_{in} = \text{arbitrary} \end{cases} \quad (2.13)$$

Which will aid us when describing the feedback paths of the OPAMP in the first approximation. The OPAMP is, in real life, quite dissimilar to this model. However, it aids us in gathering a first-look understanding of the behaviors of a circuit.

<sup>1</sup>or rather the German, even perhaps the TUM notation.

### 2.3.1 Configuration

OPAMP can be configured to have positive or negative feedback. Negative feedback is often preferred [14] in electronics circles due to being more resilient to instabilities and noise [15]. This has been theoretically described in control theory models of the OPAMP feedback path. We will refrain from explaining this approach. However, the reader is encouraged to look at Lunze's book on Control Systems [16]. There are different amplifier circuit types, such as the inverting one, which are relevant for this work and thus described below.

#### Integrator

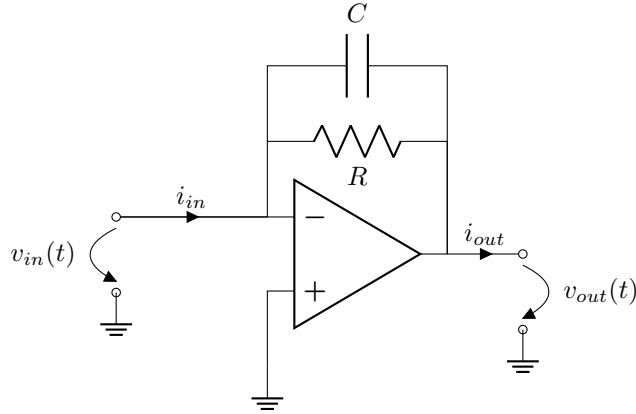


Figure 2.5: Integrator with bleed-out resistor  $R$ .

As discussed above, little to no  $R_{in}$  is provided, but an input capacity is present. We shall name this capacitor  $C_{in}$ . Keeping in mind we wish to express our small signal gain and operate in the small signal domain, we can model the GEM side as in Figure 2.6 below:

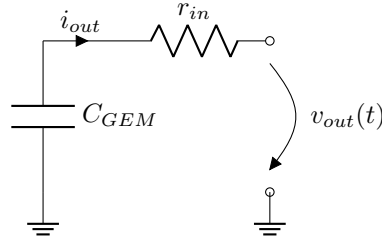


Figure 2.6: Small signal model of the GEM capacity and the minimal input resistance.

The GEM capacity and the small resistance indeed build up a time constant  $\tau$ . This is, however, negligible in our setup due to the tiny resistance of the

### 2.3. WORKING PRINCIPLE: OPERATIONAL AMPLIFIERS (OPAMP) 21

trace that leads up to our amplifier stage. However, care needs to be taken when we combine the two circuits. Namely, one can incorrectly notice  $C_{GEM}$  is building a time constant with the feedback resistor. The reason why this is incorrect is simple. Our current model explains it quite well. In a nutshell, the OPAMP behaves like an extreme resistance (remember  $i_{\pm} = 0$ ) at its inputs. Thus, isolating this time-constant behavior.

The reader might now ask why do we need the feedback resistor then? Once again, the answer lies in our circuits' practical limitations. Let us consider the unloaded, i.e., without input or output, the stationary small signal operation of our Integrator.

$$i_1 = \frac{U_{in}}{r_{in}} \quad (2.14)$$

$$Z_f = Z_c \parallel R_f = \frac{j\omega C_f + 1}{j\omega C_f R_f} \therefore U_{out} = i - i_{in} Z_f \quad (2.15)$$

$$(2.16)$$

plugging in reveals:

$$U_{out} = -\frac{U_{in}}{r_{in}} \cdot \underbrace{\frac{j\omega C_f + 1}{j\omega C_f R_f}}_{\Phi} \quad (2.17)$$

Multiplying and dividing by the complex conjugate of  $\Phi$ ,  $\Phi^* = -j\omega C_f$ :

$$U_{out} = U_{in} \left( \frac{\omega^2 C_f^2}{r_f \omega^2 C_f^2 R_f^2} - j \frac{\omega C_f}{r_f \omega^2 C_f^2 R_f^2} \right) \quad (2.18)$$

$$\therefore Gain = \frac{U_{out}}{U_{in}} = \frac{\omega^2 C_f^2}{r_f \omega^2 C_f^2 R_f^2} - j \frac{\omega C_f}{r_f \omega^2 C_f^2 R_f^2} \quad (2.19)$$

$$\therefore Re(Gain) = \frac{\omega^2 C_f^2}{r_f \omega^2 C_f^2 R_f^2} \quad (2.20)$$

$$\therefore Im(Gain) = \frac{\omega C_f}{r_f \omega^2 C_f^2 R_f^2} \quad (2.21)$$

Calculating the DC gain (for  $\omega = 2\pi f = 0$ ) yields the following characteristics. DC Gain, selected by  $r_{in}$  and  $R_f$ :  $Gain = 20 \log\left(\frac{R_f}{r_{in}}\right)$  and accompanying frequency bode plot is given. [17] Another duty of our feedback resistor is to "bleed out" the charge out of the capacitor. This builds an "integration" time constant and a recovery time constant, which we will discuss in our practical circuit.

This 20dB/dec fall indeed describes an integrating behavior. A time-domain approach can be calculated simply with the Norator model and the time response of a capacitor coupling it to the output voltage. Now, let us turn our attention to a simpler circuit that will be revealed to be robust and easier to work with.

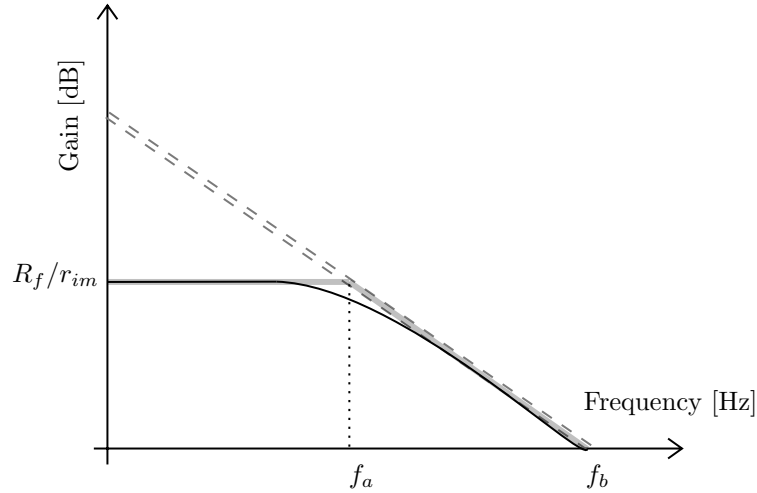


Figure 2.7: Dashed gray line: theoretical gain of only the integrator part. The black solid line is the "practical" gain considering the input and feedback resistors.  $f_a = \frac{1}{2\pi R_f C_f}$  where the so called 3dB corner frequency resides. At this frequency, the gain decreases by 20dB per decade. Finally, the unitary gain (0dB) frequency  $f_b = \frac{1}{2\pi r_{in} C_f}$  is plotted.

### Negative Gain Amplifier

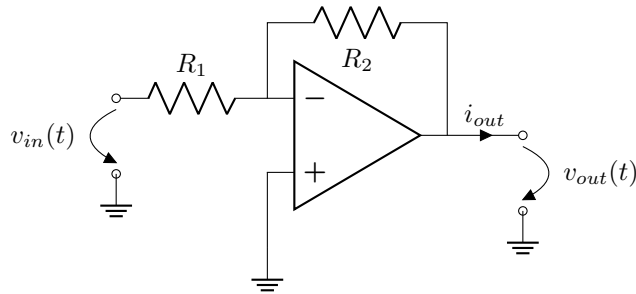


Figure 2.8: Simplest case of an amplifier. The negative gain amplifier with a  $\text{Gain} = -\frac{R_2}{R_1}$ .

Unlike many approaches in Nuclear Physics, let us try a simpler amplifier as shown in figure 2.8. This amplifier has a simple output equation using the Norton model. Thus, the output voltage is equal to the feedback path voltage

drop over  $R_2$  and described as follows:

$$i_f = i_{in} \Rightarrow i_{in} = \frac{U_{in}}{R_1} \quad (2.22)$$

$$U_{out} = -U_f = i_f R_2 \quad (2.23)$$

$$\therefore \text{Gain} = \frac{U_{out}}{I_{in}} = -\frac{R_2}{R_1}. \quad (2.24)$$

### 2.3.2 Noise

Of course, our amplifier does not magically amplify only the part we want; it also amplifies the noise we input. They also produce noise inside the integrated circuit, and any component, such as the passives, contributes to the noise by thermal causes.

#### Decoupling Capacitors

Decoupling capacitors are almost mandatory in high-frequency circuits like ours. High-frequency noise is produced via the power supply, the resistors, capacitors, and the ICs themselves, and any thermally induced noise is inflicted upon the signal. To filter this out, we require a low-resistance path for noise to escape. This can be provided with a capacitor that offers a low resistance path for higher frequency signals (since noise is very high frequency). The capacitors are connected closely to the IC's power supply pins, such as in figure 2.9, to ensure decoupling at the end IC and lower equivalent series resistance.

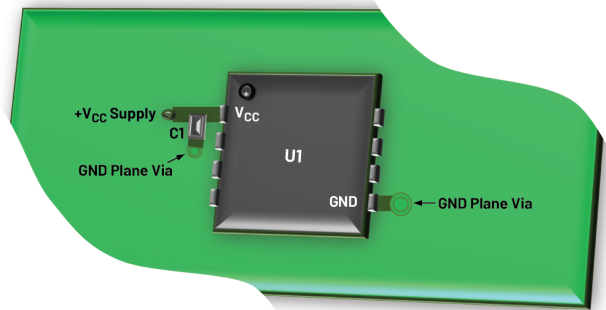


Figure 2.9: Placement of decoupling capacitors. Courtesy of **Analog Devices Inc.**

### 2.3.3 AC-Coupling

An unfortunate consequence of using optimized parts for size and price is the DC offset of the integrated circuits' output. This can be easily averted by introducing AC coupling. The easiest way is to use a capacitor to "take out" the

DC part and only allow the AC (small-signal component) part. This is evident because a capacitor is a reactance with complex resistance of  $R_C = 1/j2\pi fC$  with  $f$  being 0 (for DC), equaling infinity.

## 2.4 Working Principle: Comparators

A comparator is a special kind of OPAMP, a very high gain OPAMP -almost always saturating its output. There are two common kinds of comparators, namely open drain and push-pull. The open drain requires special pull-up resistances to output a full wave to its power supply rail, whereas push-pull does not. We investigated both of these.

The operation of the comparator is straightforward; if you input a wave into one of its inputs and supply a reference threshold to the other, it toggles between high and low output if the input waveform exceeds the threshold. A non-inverting case can be seen in the figure below.

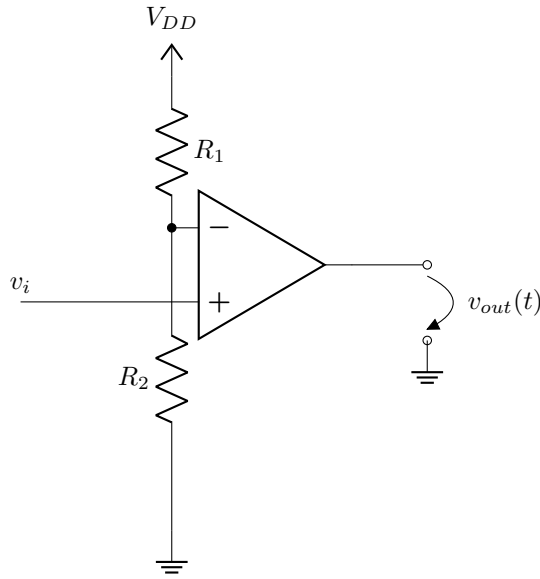


Figure 2.10: Non-inverting comparator. The threshold is set via the resistor voltage divider ( $V_{th} = V_{DD} \cdot R_2 / (R_2 + R_1)$ ) connected to the rails and the negative input. This circuit also causes a phase shift. Where its output is a bit retarded in comparison to input time.

## 2.5 Working Principle: Digitization

Having digital means to process our data is essential for this project. There is one peculiar way to achieve suitable particle identification via an energy spec-

trum, and an excellent way to have a reasonable energy resolution is to have a good timing resolution. The following subsection explains that we ensure this using time-encoded energy data.

### 2.5.1 Time over Threshold (ToT)

Different energy losses due to ionization of the gas result in different readout times and peak amplitudes. We exploit this fact in our detector. Having a comparator means we essentially have a comparator output signal dependent on the energy of the ionization. Notwithstanding the timing, this process can be calibrated using two methods. One can use a charge injector on each pad, injecting a known amount of charge, thus a known signal, and define it accordingly. Secondly, the readout can be calibrated using a known check source of a typical decay product (say  $\alpha$  decayer Am-241 or X-ray decayer Fe-55). Please refer to the figure 2.11 below.

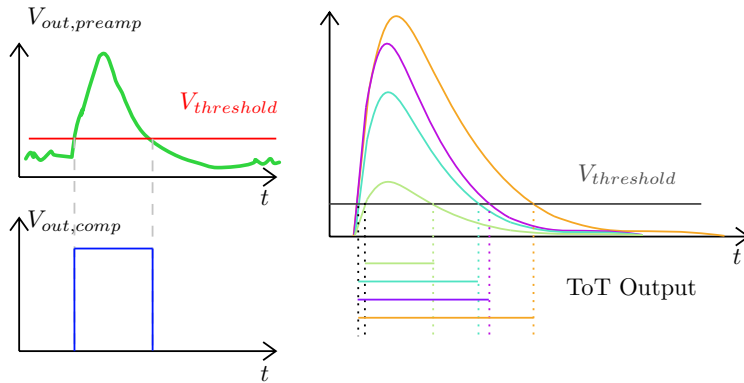


Figure 2.11: Setting a threshold (left) and different outputs of pads in correlation with peak width and height (right).



# Chapter 3

## Simulations

The theory is a safe harbor for creative thought; it allows certain things, and some does not, while restricting some parameters. This is, however, not an applicable approach when it comes to analog design. Thus, this fact led us to make some simulations. Let us further discuss these.

### 3.1 Pre-amplifier and AC-Coupling

#### 3.1.1 Integrator

We investigated the charge integrator described as section 2.3.1 via the free tool LTSpice from Analog Devices. This program allows devices from Analog Devices to be simulated. Having looked at a suitable IC, we decided to use the AD8030 as a basis for our simulations. Using the command `.step param Rf list 10k 50k 100k 500k 1Meg 10Meg 20Meg 50Meg` for a parameter sweep over the feedback resistor, we conclude the following:

1. The circuit is instantly unstable
2. The instability does not disappear for any particular combination of  $R_f$  or  $C_f$ .
3. The instability happens regardless of the input signal state.

Therefore, moving on, we had to rely on our experimental results in the Lab. We will discuss this in the next Chapter, Implementation. Let us, thus, turn our attention to a simpler circuit, the negative gain amplifier.

#### 3.1.2 Negative Gain Amplifier

Using negative amplifiers, we achieve good stability in terms of feedback. However, another reason why it makes sense to get a negative gain in the pre-amplifier is that the electron-induced signal is negative in relation to the system's

ground. If we negate, we have an output in the correct range, i.e.,  $Sig > 0V$ . This will aid us in the comparison stage.

Our simulations over different feedback resistors and feedback capacitors <sup>1</sup> yield the following graphs.

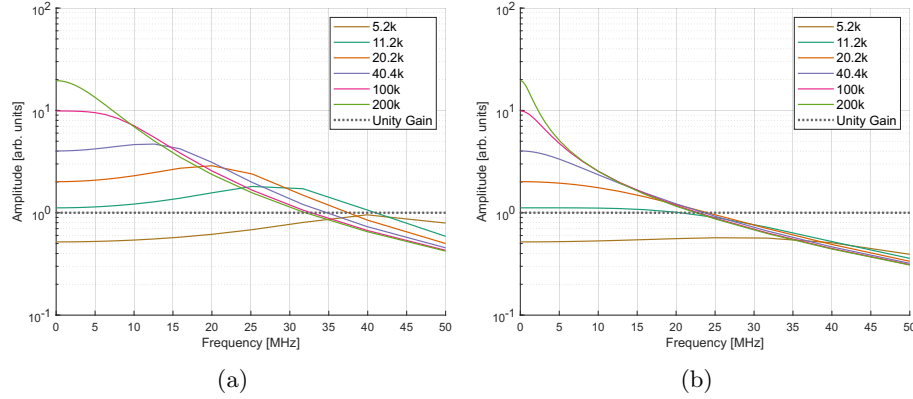


Figure 3.1: **(a)**, Frequency response plot for a feedback capacitor of 0.1pF and **(b)**, for a 0.5pF capacitor. We can see that the Gain Bandwidth Unity frequency shifts further if a lower value is used. This is due to a created system zero at an appropriate place, which coincides with the system pole of the AD8030, compensating it.

Note that the amplifier is stable for all cases, even for higher frequencies where it attenuates the signal. Unfortunately, this was not the case with our charge amplifier.

## 3.2 AC-Coupling

Before the pre-amplifier signal can be fed to the comparator, a quick fix of the offset, as discussed earlier, has to be done. The easiest way to do this is by using a resistor voltage divider with capacitive coupling. This coupling capacitor needs to be high enough to pass the signal at a range of frequencies ( $Z_c = 1/j\omega C_{couple}$ ) meanwhile minimizing Z for higher frequencies.  $R_2$  (bottom) needs to be chosen via  $\tau = R * C$  where the rise time of the output signal is set. Thus, C has to be big enough, and R has to be small enough or vice versa.

As we can deduce from the above signal simulation, the bigger the capacitor, the less attenuated the signal is. Conversely, the signal gets modulated (rise time) for higher capacitor values. A sweet spot was determined to be around 10 nF. Additionally, a resistor divider is employed in the simulation to set a DC operating point at the output. Such dividers are helpful for systems requiring a

<sup>1</sup>Required for the pole-cancellation.

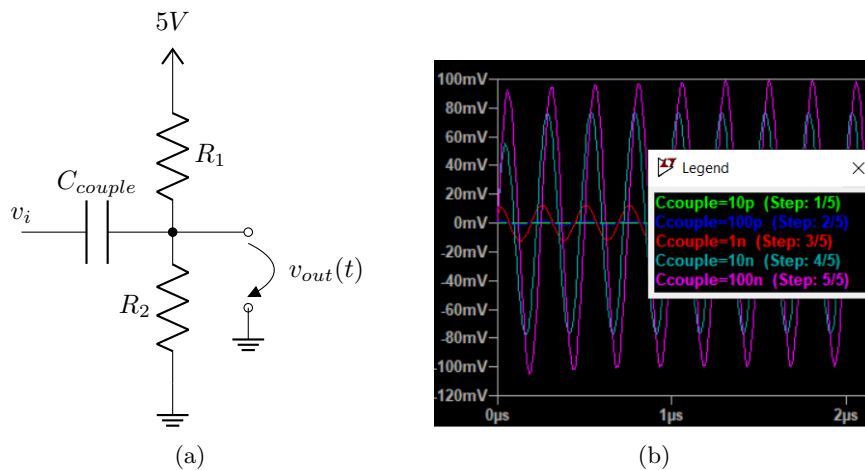


Figure 3.2: (a), The simulated circuit and (b), Plot of the  $v_{out}$  depending on the coupling capacitor.

common mode DC point to operate correctly. Such circuits are mainly digital logic circuits requiring well-defined pin states as LOW or HIGH.

### 3.3 Comparator

For the most reliable simulation model, we chose LTC6752, which offers a 2.9ns propagation delay and an input bandwidth of 280MHz when simulating. Results can be taken from the below table.

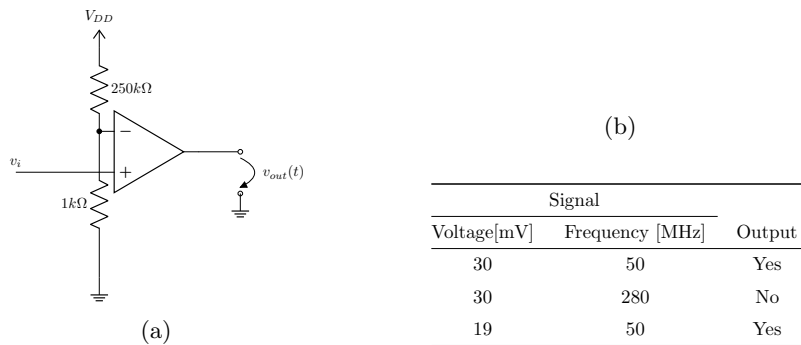


Figure 3.3: (a), LTSpice Simulation of Comparator **LTC6752** and (b), table of checks done. The threshold via the negative input is set to 19 mV.



## Chapter 4

# Implementation

*These fellas are gonna be  
ohm-less if they don't put up more  
of a resistance! [...]*

---

Dell Conagher

Having justified our theoretical background, looking through the windows of simulations, let us now, implement our circuit and have a working product.

### 4.1 OPAMP Gain Method

Our tests started with a charge-sensitive amplifier topology after the charge amplifier described in a circuit theory textbook. Nevertheless, this approach will prove to have its own caveats. That is why a more advanced topology was needed. Using a voltage follower, some of the effects of first-degree integrating feedback could be avoided. For this, we used LM310N, which we already had at hand. The LM310N Datasheet describes the following circuit.

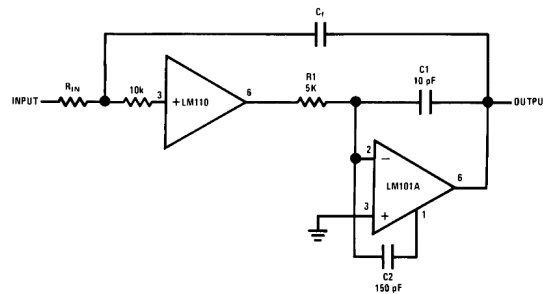


Figure 4.1: Compensation follower implemented as TL/H/7761-5 fast integrator with low input current described in LM310N datasheet.

However, the gain bandwidth of this circuit is around 600kHz, which was way too slow for an input signal of around 5MHz (slow, alpha pulse) to 7MHz

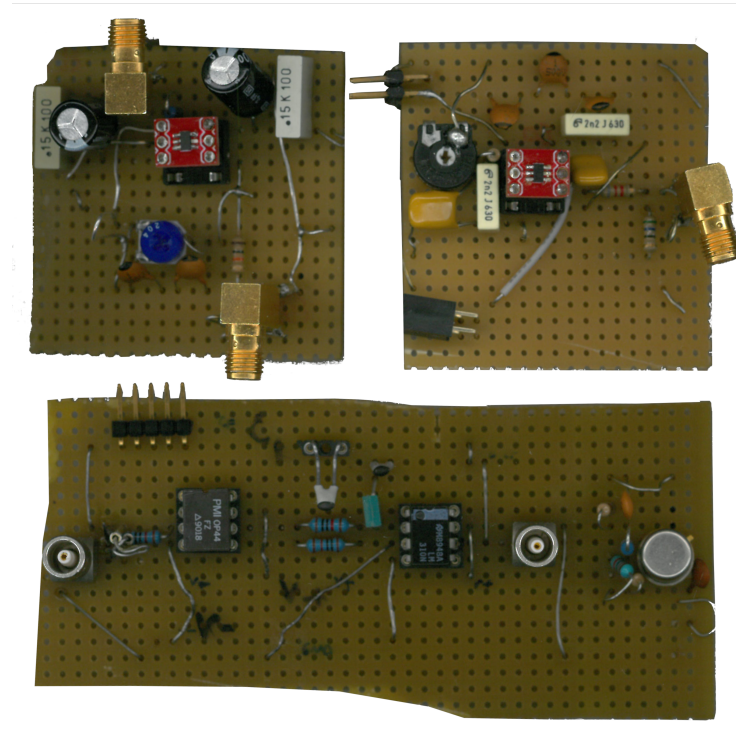


Figure 4.2: Top Left: negative gain amplifier selection board with adjustable gain (1x to 10x); Top Right: comparator speed test circuit. Bottom: preliminary charge amplifier circuit described by Figure 4.1.

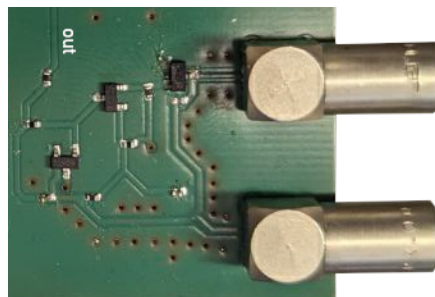


Figure 4.3: Produced PCB after Todd et al.

(fast, cosmic ray)<sup>1</sup>. Therefore, a more advanced topology was needed. A literature search yielded the paper written by Todd et al. [18]. This paper describes a JFET-input BJT difference stage amplifier to be operated at low temperatures.

<sup>1</sup>Observed experimentally using an ORTEC pre-amplifier and confirmed with our amplifier on figure 4.5.

The choice of JFET input is due to its good noise performance. We followed through and a PCB at figure 4.3 was produced. This circuit worked up until 50MHz and provided ample DC gain. However, we decided against it since the circuit produced a massive signal shift.

Having 64 channels to measure, considerations about stability, per channel price and ease of use had to be made. The unstable tendencies of an integrator led us to the simple topology of a negative feedback amplifier as we described in the previous chapters.

The circuit required enough unitary gain bandwidth (BW). This parameter is specified in the datasheets, giving the designer an idea about the circuit poles and zeroes. We tested these using a calibrated VNA measuring the amplitude of the  $S_{21}$  parameter seen in figure 4.4. The selection was also done using the unit prices seen in table 4.1.

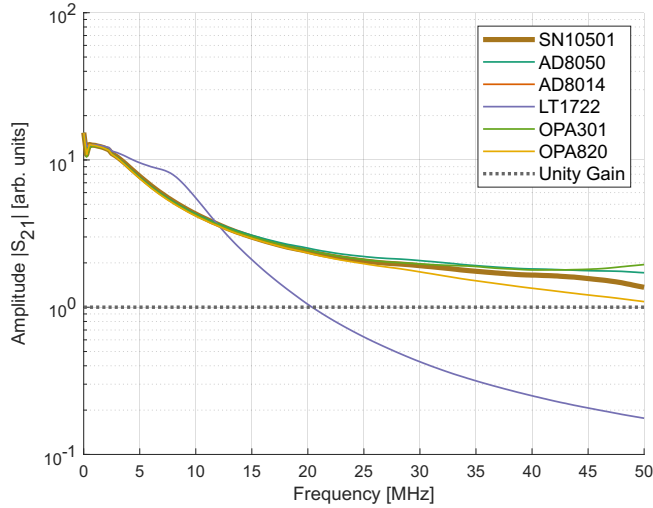


Figure 4.4: Amplitude Plot of  $S_{21}$  of the tested circuit (top left) at figure 4.1.

Having considered the above options, the ideal solution (gain per price at 30MHz) was the SN10501DBVT by Texas Instruments. Figure 4.5 shows the preliminary result of our amplifier selection, having a gain of at least 30 times the input. The input waveform is produced by a test GEM chamber using a double-stacked GEM configuration. Unlike our simulations, the gain is at least 2 to 3dB higher than the expectation, owing to the feedback path's high equivalent resistance due to the feedback capacitor of 0.5 pF.

### Noise Filtering

All real components generate some noise, which can cause problems if not properly managed. When using high-gain amplifiers, it's important to filter out the

Table 4.1: Amplifier Selection Table. The price is given per 100 units. Unity Gain Bandwidth advertised and measured (via the top left circuit of figure 4.2) gain bandwidth. OPA365AIDBVR was unstable, yielding no measurable bandwidth.

Amplifier	Price [€]	Unit Gain BW [MHz]	Measured BW (4.4) [MHz]
SN10501DBVT	72.70	100	$\geq 50$
LT1722CS5	214	200	20
AD8055ARTZ	214	300	$\geq 50$
OPA820IDBVR	199	240	$\geq 50$
OPA301AIDBVT	182	150	$\geq 50$
OPA365AIDBVR	145	50	-

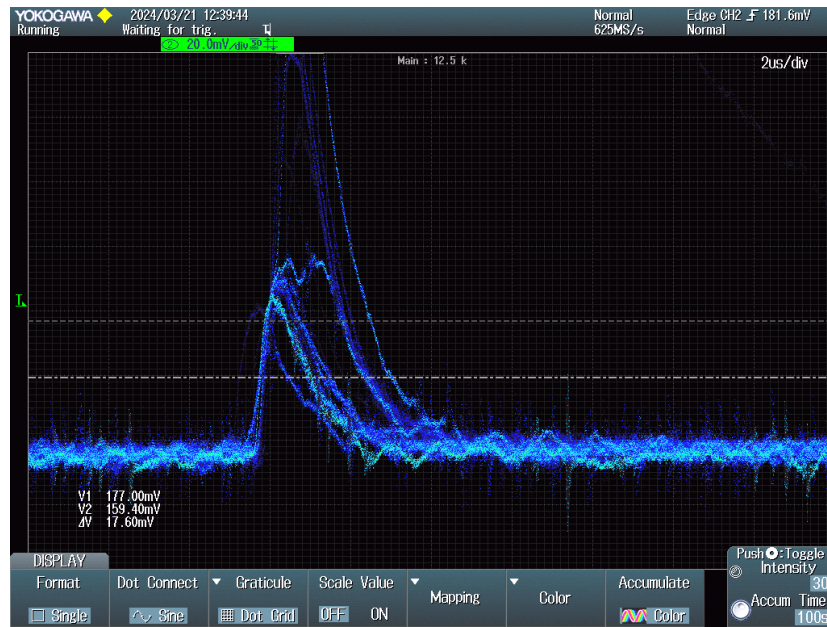


Figure 4.5: Oscilloscope plot of the output waveform (tones of blue) collected over a few seconds. We see the proper induction pattern produced by the GEM chamber anode.

noise from the power pins. If this noise isn't dealt with, it can cause instability and add unwanted harmonics to the output. Ergo, multiple filtering capacitors had to be put parallel to the DC power supply pins, ensuring low series parasitic resistance in comparison to GND.

### 4.1.1 AC-Coupling

The SN10501 offers a  $3\mu\text{A}$  input bias current and a  $100\text{nA}$  input offset current at room temperature. This effect leads to the shifting of the output via the set negative DC gain factor via the resistors times the output load resistance. Such an offset is called a DC big signal part of our output signal. This was easily defeated via an AC coupling using a suitable capacitor. The capacitor once again determines the signal rise time with the output load,  $\tau = R \cdot C$ . This circuit behaved almost identically to our simulations.

### 4.1.2 Comparator

Preliminary tests with socketed DIP IC yielded unsavory results at the output; the signal was too fast for the comparator. Thus, a similar search, such as the amplifier, was performed for the comparators. Many examples were bought of SOT-23-5 packaged ICs, and tested via the following test circuit.

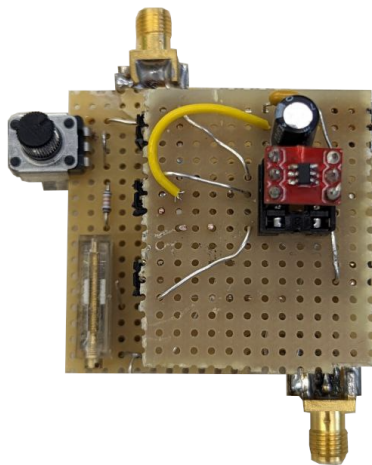


Figure 4.6: Circuit made to have coarse (black potentiometer) and fine (transparent potentiometer) threshold adjustment to test the comparators bought.

It is indeed hard to quantify how well a comparator works, in this case we sufficed with an oscilloscope measurement showing the signal group delay and the output swing of the comparator. In addition, the price of the comparators was essential, just like the amplifier selection. Having produced the test circuit at 4.6, several of the ICs were tested for a given threshold we arbitrarily chose in regard to our amplifier-produced test signal. The main candidate was Microchip Inc. MCP6561RT-E/OT, which offered a competitive price for a fast comparator that fulfilled our requirements.

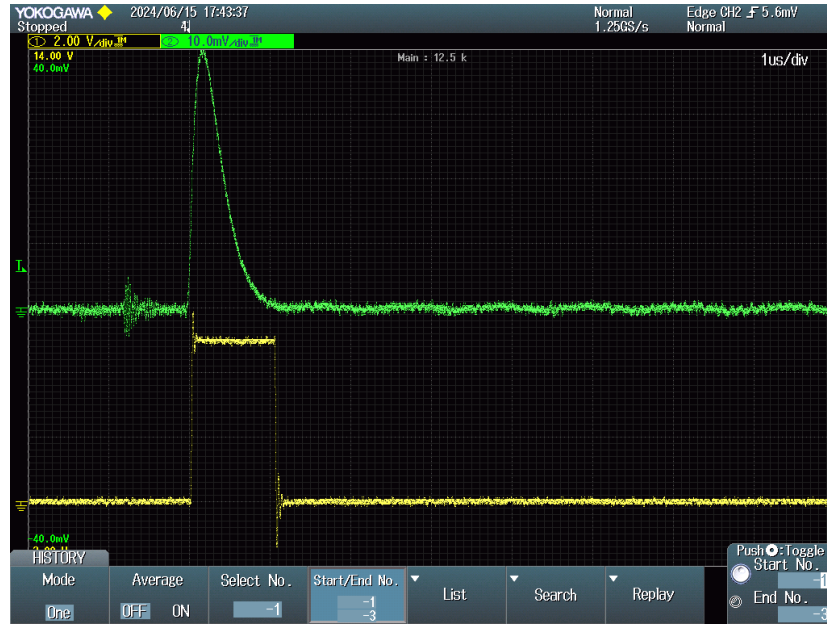


Figure 4.7: Oscilloscope plot of the output (yellow) waveform of the comparator in comparison to the input (green) waveform produced by the amplifier stage before. A measurable phase delay is present, as well as a small back EMF-caused signal to noise at the input when the comparator outputs.

## 4.2 Digitization

Numbers. Without numbers, we cannot quantify and measure the world around us. Therefore, it is of utmost importance that we collect our data and represent them in numbers. Thus, a digitization<sup>2</sup> method to quantize the comparators' output needed to be developed. Turning our head to fast digital readout, thinking a polling rate of 500kHz per channel would be enough, we started to implement a fast readout code for the Arduino family of microcontrollers. Using a microcontroller is essential because it provides real-time processing of the data, unlike a processor, e.g., Raspberry Pi.

### 4.2.1 Arduino Studies

This microcontroller board has a 16MHz clock onboard, which theoretically should allow us to read our comparator output with no buffers or active components in between. To investigate, we wrote the following code snippet.

The following code snippet allows for 1.25 kbyte/sec transfer rates, which means through the baud rate 20Mbits/sec is produced, within a 8 bit data is sent out, with 2 bytes for the PORTB contained word plus the line feed character.

<sup>2</sup>any of the numerals, especially when forming part of a **number**.



The flip-flop circuit seen in above figure 4.8 works as such: The input L goes high (as does D), while a clock signal rises the CLK input high, causing the output Q to toggle. While the Q toggles, the input L along with Q toggles the first AND gate on. Simultaneously, the D pin of the second and third flip flop is turned on at the same clock cycle, turning on the secondary Q and ternary Q while the 3-fan in OR gate is turned on. A certain propagation delay is added to each flip-flop, resulting in a delay of turning each Q off by a few delay times (intrinsic to the flip-flop). For example, the signal stays high since one Q being high is enough for the output to stay on. After three propagation delays, the output turns off. This essentially stretches the signal with the initial signal on time  $t_{in}$  with three propagation delays:  $t_{in} + 3\tau_{flipflop}$ .

We tried the above flip-flop approach [20] at figure 4.8, however, while having a great stretching ratio proportional to the input waveform, this method required very high clock signal to function as well as many flip-flops to implement. Given our discrete nature of the circuits, this was practically impossible to implement for 64 channels on a PCB. Thus, we had to look for the third solution, the mono-stable.

## 4.2.2 Mono-stable and the Binary Hit Mode

Thinking about ease of design and costs, we face, perhaps, the most well-known IC - the 555 Timer IC by Signetics Inc. This IC can be configured in many ways, as an oscillator (astable) or as a time pulse-producing circuit (mono-stable). The time of the output pulse is determined via the RC network connected between Vcc, Discharge (dis), and Threshold (th) pins of the IC<sup>3</sup>.

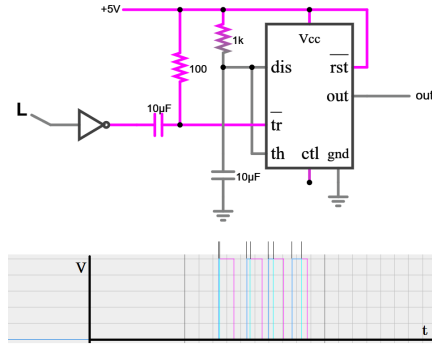


Figure 4.9: The famed NE555 Timer IC is configured to accept positive pulses of 5V and output at its mono-stable operating point for a determined output time of 0.011 seconds. Various input durations (blue and thin) cause the same output (pink and thin) duration, causing the initial energy resolution to be lost.

Having only one stable point means it only operates at that point. This

<sup>3</sup>to no one's surprise, it is calculated once again via  $\tau = R \cdot C$

completely removes the wished energy resolution achieved by the time over threshold method described in the intro and implemented via the comparator circuit. Such with our mono-stable circuit now, we shall still operate in the "Proportional" region but behave more like a yes or no binary counter described by figure 2.2's Geiger region. However, the entire detector still would have a granulated position output and only a Geiger-like counting for each 8x8 channel.

To overcome this issue of losing energy resolution, we have devised a plan. We shall explain this in detail in the following section.

### 4.3 One channel to Multiple Channels

It was time to put all the pieces together and treat it as a single channel with the complete signal processing chain. Our anode is segmented into an 8x8 grid of copper pads. Each 8x2 matrix of such pixels creates a 16-channel cluster to which a readout PCB is connected.

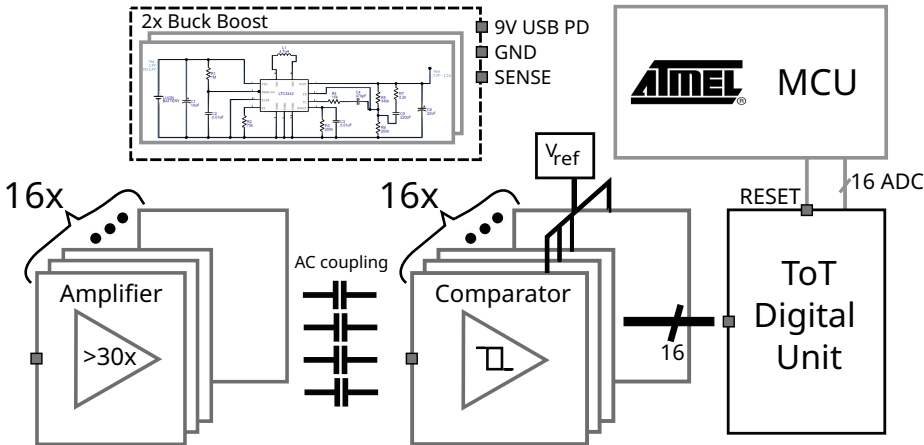


Figure 4.10: Proposed read-out chain for boards supporting a 16-channel amplifier, a Schmidt-trigger-like comparator, and a subsequent digitizing pair of a time over threshold quantifier and a real-time readout via an Atmel Microcontroller Unit. Based on these proposals, only the amplifier board is currently working as intended.

Before trying a 16-channel readout board as suggested by figure 4.10, we decided it would be a good idea to prove that our readout method works as intended for a singular channel. Therefore, we ordered the following board and produced the following test setup.

The PCB in figure 4.11 was put in a metal box with multiple LEMO connectors connected throughout the different parts of the signal chain to enable us to measure different parts of the signal in real-time with an oscilloscope. This box was also grounded with the circuit ground and the power supply ground. This grounding was also connected to the detector chassis indirectly while testing.

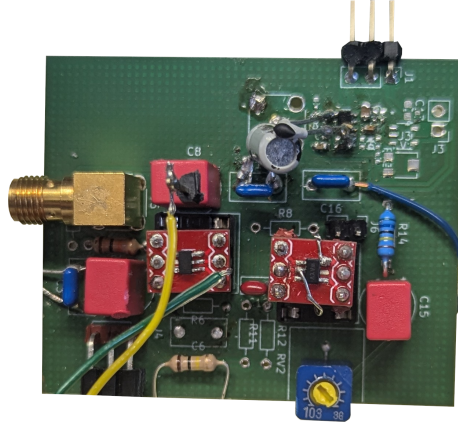


Figure 4.11: PCB designed to test a singular analog front-end channel. This PCB was confirmed working.

After confirming its full operation, we turned our attention to the 16-channel boards described by figure 4.10. It took us a long time to solder them per hand and debug the physical issues. To note was the following: the gain factor was different from the test circuit, and initially, this was thought to cause problems.

One particular instance was while measuring the readout, despite having the results for a singular channel board at figure 4.11, the 16-channel PCB seemed to have no output despite having the exact layout on a channel basis. The issue was speculated to be the gain bandwidth getting decreased or even the feedback path building a stray filter with the internal layers of the PCB. Frustrated and looking for answers, our trusty VNA was required once more to confirm.

Measured	$C_f$ [pF]	$R_f$ [k $\Omega$ ]	Corner Frequency [MHz]	DC Gain	Bandwidth [MHz]
1	0,5	91	3.5	9.1	$\approx 5$
3	$\approx 0$	180	885	18	$\approx 10$
5	$\approx 0$	180	885	15	$\approx 25$
6	$\approx 0$	390	409	11	$\approx 10$
10	Single Channel Benchmark Circuit			10	$\approx 25$

Table 4.2: Table of some conducted measurements with different gain configurations. Bandwidths are given approximately, and the corner frequency is calculated via  $f_C = 1/R \cdot C$ .

Having these results, it was time to test the circuit with our detector. Nonetheless, this was futile since the amplifier card did not produce any signal. It was after thorough consideration that we found out what the error was. The detector was not grounded, and the circuit ground and the chassis ground were not connected. Deploying a ground connection solved our issue and gave us a

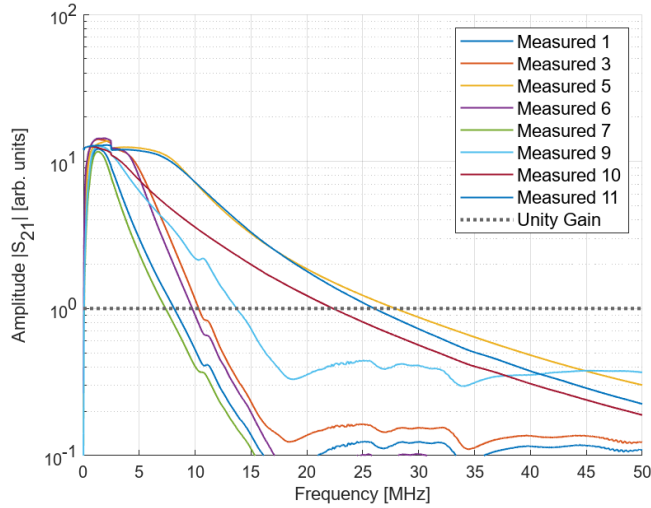


Figure 4.12: Measured arbitrary amplitude plot of the different feedback configurations of the 16-channel board. Three major traces are of interest: Measured 1, where the 16-channel board was measured as-is, one-channel test board's measured trace, Measured 10 (benchmark); and finally, the best bandwidth and gain offering configuration, Measured 5. The configurations can be taken from the table4.2

signal. A side effect of the VNA experiments was the effective optimization of the gain for the best gain bandwidth ratio seen in figure 4.12 and table 4.2 and was thus not entirely futile. Thereby, now with the ground connected, the card functioned with no error. Let us discuss figure 4.13, which has the results of our measurements.

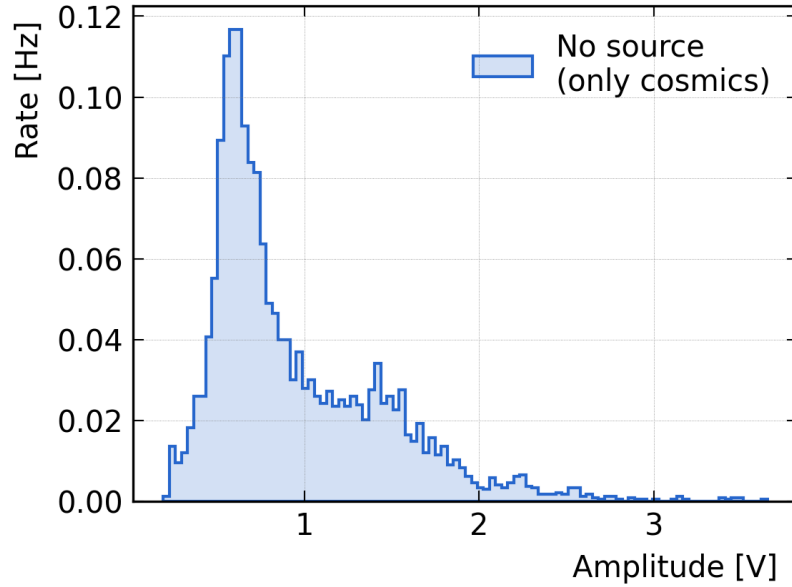


Figure 4.13: Processed data of 5000 particle events and their rate per second versus the produced signal amplitude.

We clearly see a peak around 0.5 Volt amplitude. This peak is caused by the so-called Minimum Ionizing Particles. MIPs are a type of cosmic rays. The reason why these particles are minimally ionizing is because of the results of many layers of building on top of the measurement setup. This phenomena of reducing the energy of incident particles is explained by the Bethe-Bloch formula<sup>4</sup>. Here, depending on the relative speed of the particle  $\beta = c/v$ , the effects of energy loss differ in terms of their dominance See the figure ?? [10] Other parts of the plot is theorized to be caused by background radiation of the setup, room or the involved materials.

After providing these data, our attention was turned to our comparator card. The fully assembled card also did not function. Its outputs were always high, and no matter what the input signal was, it never returned to low. We speculate that the card did not function due to a parasitic effect bound by the multi-layer construction of the PCB. Below is a fully assembled card.

<sup>4</sup>Describing the particles passing through material.

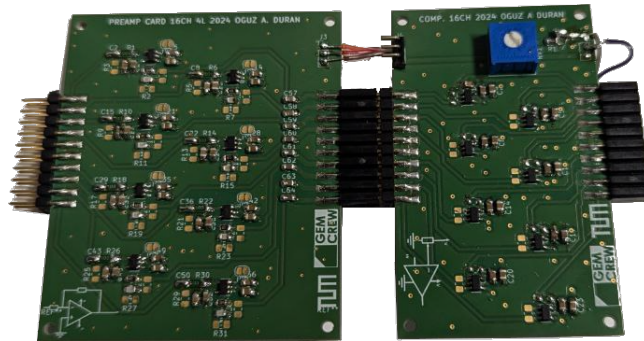


Figure 4.14: Left, fully assembled amplifier card, right, fully assembled comparator card.

Despite our extensive efforts, the comparator card did not function as intended. No matter what the input state of the threshold set was, the output was always high. This was quite confusing since it was a 1:1 copy of the one channel test circuit we produced, which functioned with no problems. We did not have enough time to fix this issue for the time frame of this thesis.

The final piece of the puzzle was the monostable card. We designed this card using the famed 555 timer and an inverter for the input such that the 555 could be used in a monostable configuration because that required a falling edge from a high signal to function. This PCB was, however, not ordered and not tested due to the lack of time. Below is a rendering of the final PCB.

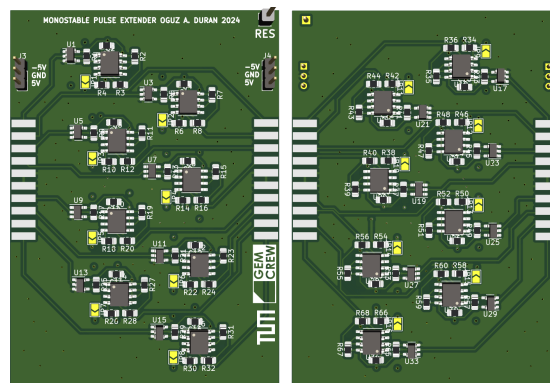


Figure 4.15: 3D rendering of the monostable card based on the 555 IC.

## 4.4 PCB Layers and Description

We now describe the workings of the PCBs. The cards are designed to be as modular as possible. They share multiple qualities like having an male input header and female output header positioned in the same X coordinate and having an equal height dimension. Furthermore they also share a power bus at the same Y coordinate on each input and output sides of the cards. This allows the cards to freely cascade.

First, let us inspect the amplifier card we produced. This board consists of four layers. The TOP layer has the first 8 channels. One layer below, the IN1 layer is used for power distribution only having traces for the -5V and 5V supply rails. Moving on, the IN2 layer's only purpose is to isolate the top and bottom from capacitive coupling by offering a path to ground.

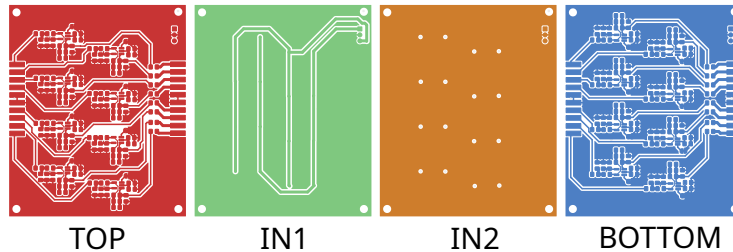


Figure 4.16: From left to right: stack-up of the amplifier board layout done in KiCAD.

One peculiar aspect of the board is the fact that the top and bottom amplifiers are ever so slightly moved from each other to disallow any resonances or capacitive couplings to occur. The same idea was kept in consideration when placing ground stitching vias between the layers. This board only has one power header facing towards the output since it does not need to supply power to the GEM anode. Another consideration is the connecting ground pins of the input header. This connects the system - power supply, read-out chain etc.- ground to the GEM ground and chassis.

Let us now move to our comparator card. Similar considerations like the amplifier board were done to reduce parasitic effects and coupling. One feature of the comparator card is the global voltage reference it uses to compare against. This is done via a Trimpot connected to the 5V supply via a voltage divider. This card also supports chaining the power rails. The layer IN1 is used for distributing the 5V power and the layer IN2 is used to distribute the reference voltage.

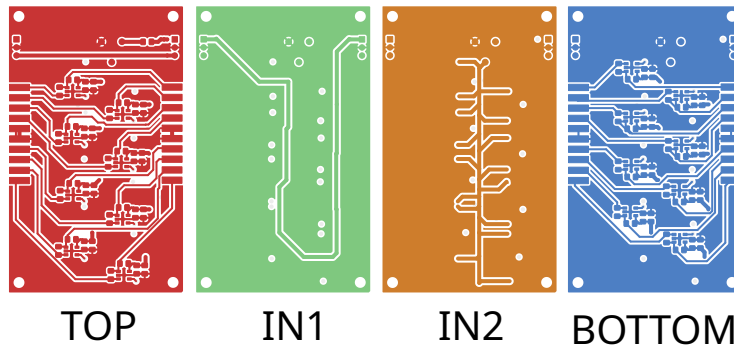


Figure 4.17: From left to right: stack-up of the comparator board layout done in KiCAD.

Additionally each of these boards are adorned with a small artwork of the function it takes.

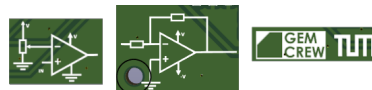


Figure 4.18: Ornaments and visual cues to the board's functionality. GEMCrew nad TUM's Logo.

All boards also support a M2 screw hole in each corner to make mounting easier. Let us now take a look at our final board we produced, the LEMO-connector signal collecting board. This board connects internally the 16 channels at its input. It has pin headers where jumpers can be set to select what channel shall be connected together. Its last feature is the pads to solder capacitors or diodes for either captive coupling or a isolated coupling of the each channel to the output.

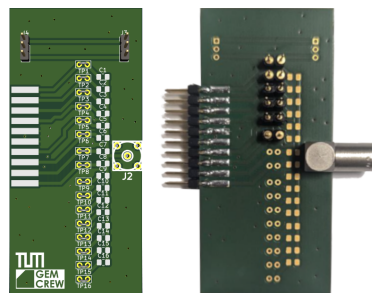


Figure 4.19: 16-Channel LEMO Connector adapter board.

This circuit is only two layers. It is a relatively simple design where only

the pins are connected and it has no active components (if only used for AC-coupling).

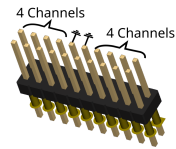


Figure 4.20: 10x2 Pin headers used for the boards.

Lastly, we give the pin header configuration we used for our cards, which corresponds to the connections on the GEM anode. It has 4 channels, then two ground pins then 4 channels on one side. It is mirrored perfectly on the other ten pins.

## Chapter 5

# Summary and Outlook

In this thesis I described my journey of developing a readout system for a GEM based detector which will be used for scientific outreach. I outline my approach to circuit design by first theoretically motivating my hypothesis, then using common prototyping methods to have a working prototype to compare against my hypothesis, and lastly producing a working product which is highly expandable and flexible to work with. Not only this, but also the entire system is modular and made using off-the-shelf parts, unlike some implementations with FPGAs and ASICs.

Furthermore, tests are done on the end product to assure its functionality. Insights are then gathered from the working part of the amplifier card. These insights enlist several aspects of the detector. A main aspect we wish to emphasize is the detection of numerous particles. Given data, we propose and motivate why several different particles could be detected.

Leaving aside the product aspect, this thesis enabled me to delve into the realm of analog electronics. I learned many techniques that will not ever be covered in any textbook, and could only be attained perhaps through listening to older analog design engineers - but without doing so. Working in such an interdisciplinary topic gave me real insights of working with other disciplines and their people. I learned how to approach a given physical entity and problem and solve it through the glasses of an engineer. Additionally, I was given the chance to learn how to explain such different and practical topics to many people in particle physics.

Last but not least, I wish to emphasize that the outreach aspect of this detector is a personal matter to me. I was not given a chance to look through the window of science when I was a teenager, therefore, it is a duty of mine to provide such to the next generations. I believe early contact with real world cutting edge physics and engineering is a great way to motivate children to pursue degrees and education of said fields.

## 5.1 Outlook

Despite our countless efforts, love, and labor intensive man-hours poured into this project; it is far from complete. For instance, the 64-channel readout system via the comparators are not functional. Additionally, despite drafting and trying ideas about digitizing our signals, none could be developed fully. As a result, entire part of displaying gathered track and data had to be left out. Therefore, it would be the most important to finish these efforts to have a complete package of this outreach detector.

I plan to be involved with the further development of this project, not only in the engineering related part, but also the subsequent outreach that needs to be done in schools. I wish to share my passion and knowledge with young adults and hope to leave a positive impression and a yearning for science in their minds.

## 5.2 Acknowledgments

I hereby thank wholeheartedly to Berkin Ulukutlu, without whom, this project will not have taken place. He was a comforting and wise guide throughout this thesis and working with him was very pleasant. He shared a similar passion for detectors and physics as I do, which bridged our goals together and made us a iconic duo.

Another person I owe my thesis and subsequent degree is, Prof. Dr. Gabriele Schrag. She held my hand when I needed it the most and helped me get through difficult times in my academic career. For this and for her kind, compassionate and understanding approach to each of her own students; I owe her a great thank you.

Lastly, I wish to thank my family and friends, who all believed in me and stood behind me in my lowest times where I doubted myself.

**Thank you!**

# Appendix

We give the following plot for reference.

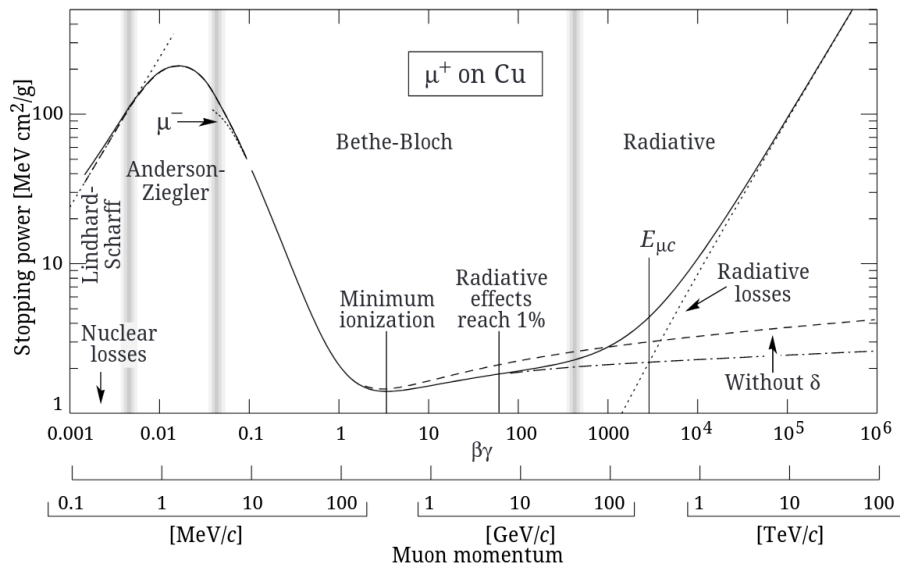
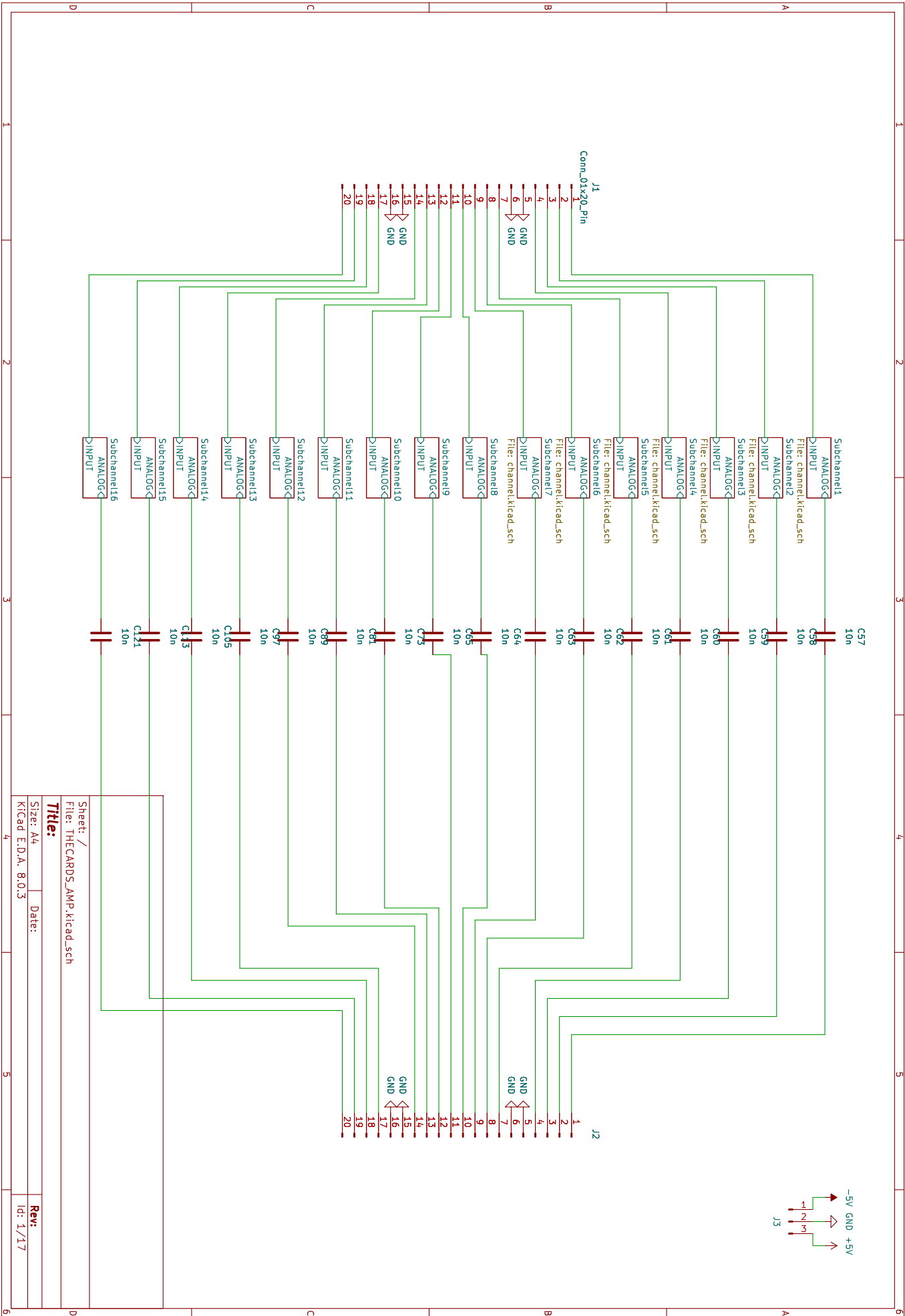


Figure 5.1: Data below the break at  $\beta\gamma \equiv 0.1$  are taken from ICRU 49. Source for the plots, **Veyssiere et al., Nucl. Phys. A159, 561 (1970)**

## Schematics

The Schematics for the designed circuitry is attached.



Sheet: /  
 File: THECARDS\_AMP\_kicad\_sch

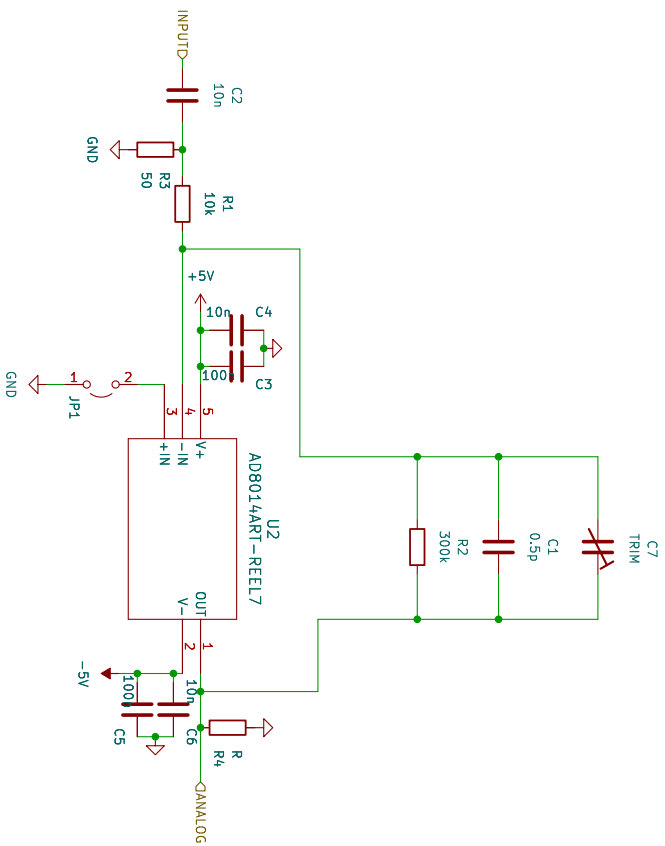
**Title:**

Size: A4 Date:

KiCad E.D.A. 8.0.3

**Rev:**

Id: 1/17



Sheet: /Subchannel1/  
 File: channel.kicad\_sch

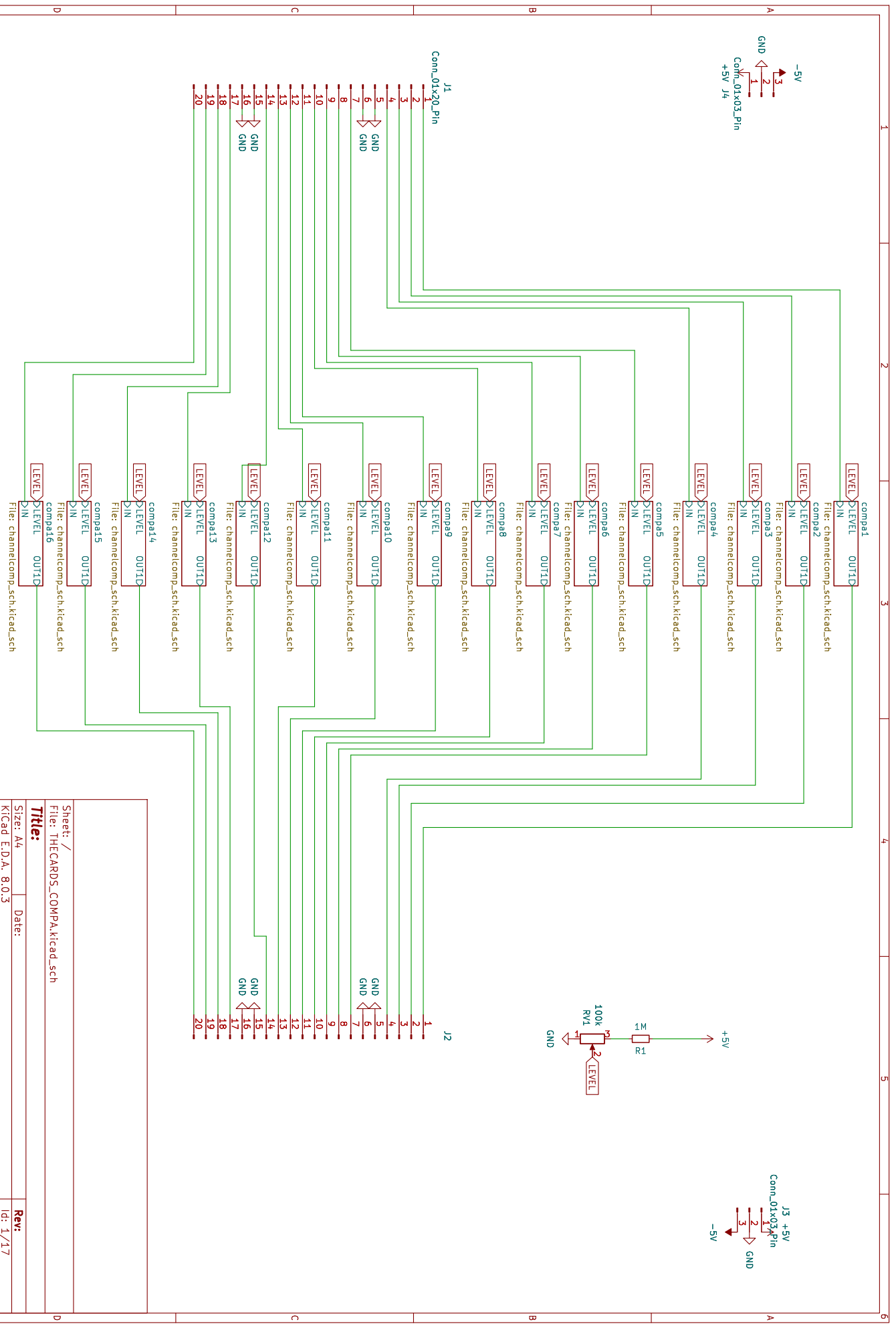
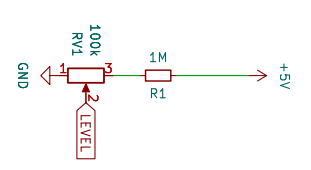
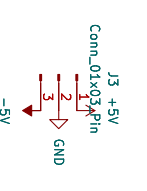
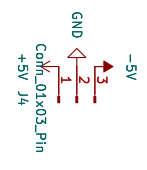
**Title:**

Size: A4 Date:

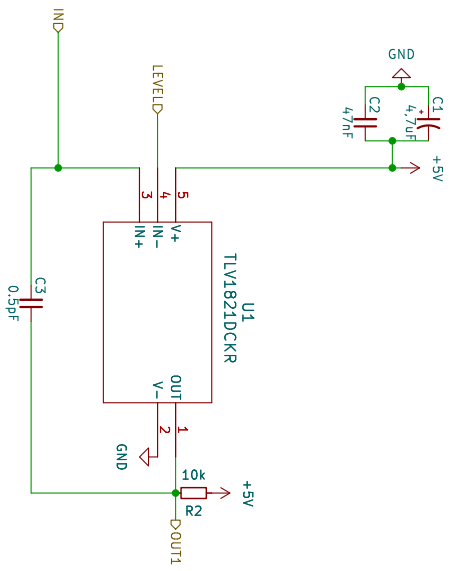
KiCad E.D.A. 8.0.3

**Rev:**

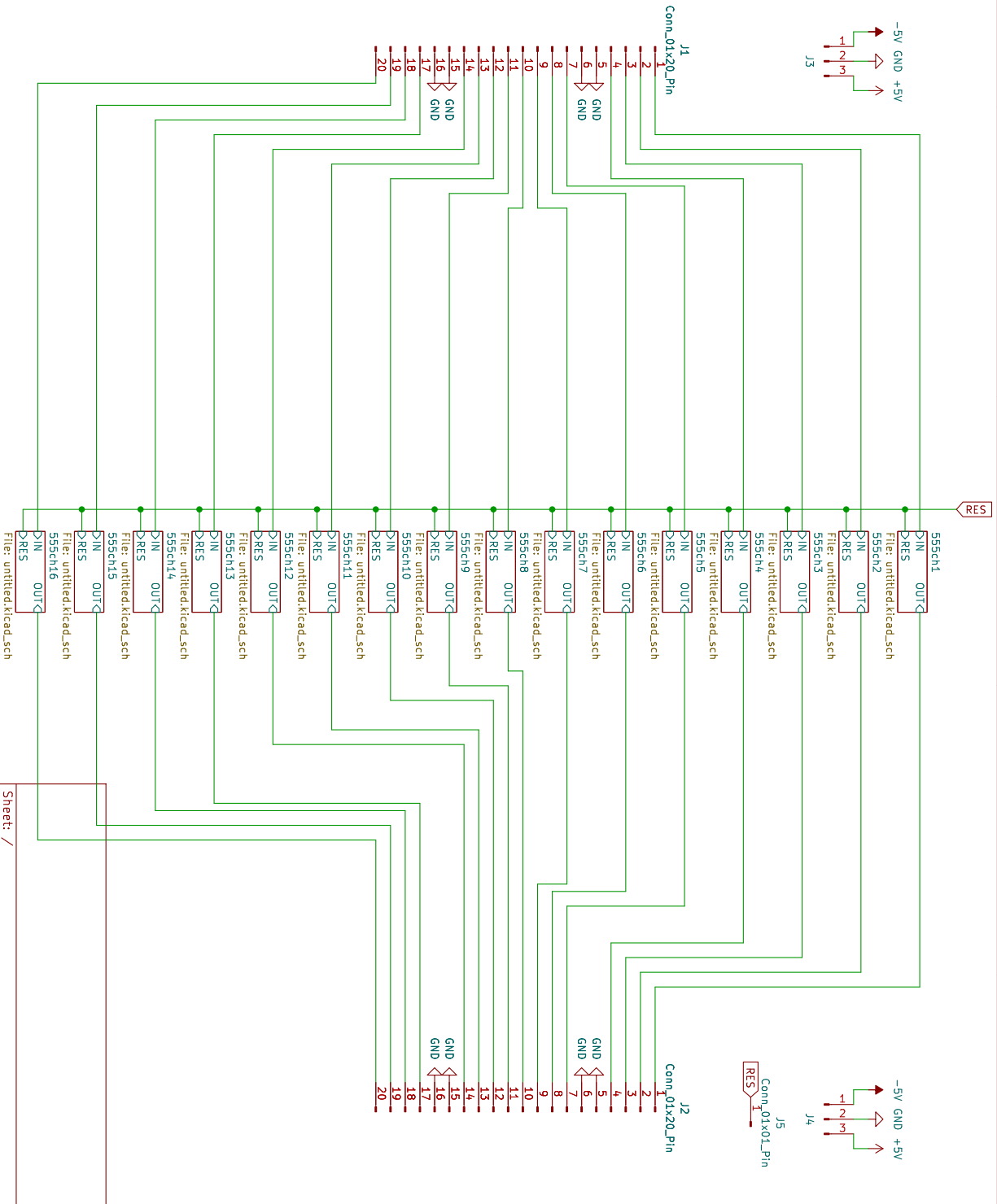
Id: 2/17



Sheet: /	
File: THECARDS_COMP.kicad_sch	
<b>Title:</b>	
Size: A4	Date:
KICad E.D.A. 8.0.3	
Rev:	Id: 1/17



Sheet: /compa1/	
File: channelcomp_sch.kicad_sch	
<b>Title:</b>	
Size: A4	Date:
KICad E.D.A. 8.0.3	
	<b>Rev:</b>
	Id: 2/17



Sheet: /  
 File: THECARD\_555MONO.kicad\_sch

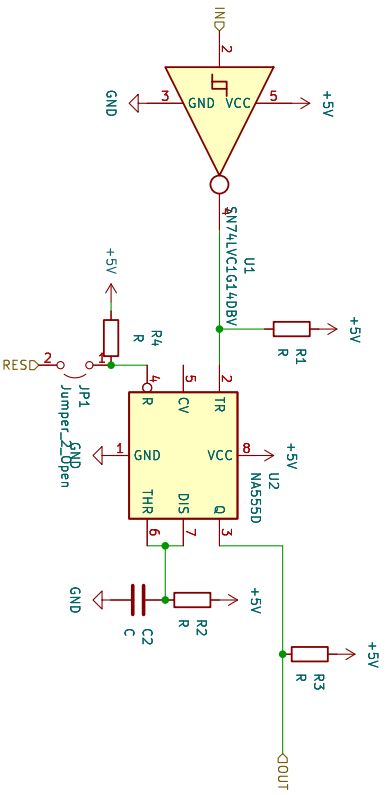
**Title:**

Size: A4 Date:

KiCad E.D.A. 8.0.3

**Rev:**

Id: 1/17



Sheet: /555ch1/  
 File: untitled.kicad\_sch

**Title:**

Size: A4 Date:

KiCad E.D.A. 8.0.3

**Rev:**

Id: 2/17



# Bibliography

- [1] F. Becchetti, “History of the bubble chamber and related active- and internal-target nuclear tracking detectors,” Nuclear Instruments and Methods in Physics Research Section A: Accelerators, Spectrometers, Detectors and Associated Equipment, vol. 784, pp. 518–523, 2015. Symposium on Radiation Measurements and Applications 2014 (SORMA XV).
- [2] W. Bothe and W. Kolhörster, “Das wesen der höhenstrahlung,” Zeitschrift für Physik, vol. 56, p. 751–777, Nov. 1929.
- [3] G. F. Knoll, Radiation Detection and Measurement. Brisbane, QLD, Australia: John Wiley and Sons (WIE), 3 ed., Jan. 2000.
- [4] S. Benson, Searching for CP violation in the  $B^0_s \rightarrow \emptyset\emptyset$  decay at LHCb. PhD thesis, 06 2014.
- [5] I. Balossino, “Operation and readout of the cgem inner tracker,” 05 2022.
- [6] P. Hauer, “The upgraded ALICE TPC,” Nucl. Instrum. Methods Phys. Res., A, vol. 1039, p. 167023, 2022.
- [7] A. C. at CERN?, “The upgrade of the ALICE TPC with GEMs and continuous readout,” JINST, vol. 16, no. 03, p. P03022, 2021. 88 pages, 60 figures.
- [8] H. Hernández, B. C. de Souza Sanches, D. Carvalho, M. Bregant, A. A. Pabon, R. W. da Silva, R. A. Hernandez, T. O. Weber, A. L. do Couto, A. Campos, H. A. Cubas, T. A. Martins, M. G. Munhoz, and W. Van Noije, “A monolithic 32-channel front end and dsp asic for gaseous detectors,” IEEE Transactions on Instrumentation and Measurement, vol. 69, no. 6, pp. 2686–2697, 2020.
- [9] L. Bugia, “Characterization of a multi-channel-thgem detector for photon detection,” 2023.
- [10] W. R. Leo, Techniques for Nuclear and Particle Physics Experiments: A How-to Approach. Springer Berlin Heidelberg, 1994.
- [11] H. Raether, Electron Avalanches and Breakdown in Gases. Butterworths advanced physics series, Butterworths, 1964.

- [12] W. Blum, W. Riegler, and L. Rolandi, Creation of the Signal, pp. 1–24. Berlin, Heidelberg: Springer Berlin Heidelberg, 2008.
- [13] H. F. Mayer, Ueber das Ersatzschema der Verstärkerröhre, vol. 15, p. 335–337. Springer, 1926.
- [14] S. Becker, “The stability factor of negative feedback in amplifiers,” Proceedings of the IRE, vol. 32, no. 6, pp. 351–353, 1944.
- [15] “Basics of Operational Amplifiers and Comparators,” Toshiba Corporation, 2020.
- [16] P. D. J. Lunze, Regelungstechnik 1: Systemtheoretische Grundlagen, Analyse und Entwurf einschleifiger Regelungen. Springer Berlin Heidelberg, 2020.
- [17] Linear Circuit Transfer Functions: An Introduction To Fast Analytical Techniques. Wiley, Apr. 2016.
- [18] A. R. Todd, A. W. Alexander, and M. F. Jarrold, “Implementation of a charge-sensitive amplifier without a feedback resistor for charge detection mass spectrometry reduces noise and enables detection of individual ions carrying a single charge,” Journal of the American Society for Mass Spectrometry, vol. 31, no. 1, pp. 146–154, 2020. PMID: 32881508.
- [19] K. Park and J. Park, “Time-to-digital converter of very high pulse stretching ratio for digital storage oscilloscopes,” Review of Scientific Instruments, vol. 70, pp. 1568–1574, 02 1999.
- [20] J. Szydwczyński, D. Kościelnik, and M. Miśkiewicz, “Time-to-digital conversion techniques: a survey of recent developments,” Measurement, vol. 214, p. 112762, 2023.